Novel safety evaluation technique for ships in offshore anchorage under rough seas conditions for optimal ship routing

Lee, Sang-Won

Sasa, Kenji

Chen, Chen

Waskito, Kurniawan T.

Cho, Ik-Soon

(Citation)
Ocean Engineering,253:111323

(Issue Date)
2022-06-01

(Resource Type)
journal article

(Version)
Accepted Manuscript

Novel safety evaluation technique for ships in offshore anchorage under rough seas conditions for optimal ship routing

Sang-Won Lee[*], Kenji Sasa[*1], Chen Chen[**], Kurniawan T. Waskito[*], and Ik-Soon Cho[***]

* Graduate School of Maritime Sciences, Kobe University, Kobe, Japan
** School of Navigation, Wuhan University of Technology, Wuhan, China
*** Division of Navigation Convergence Studies, Korea Maritime & Ocean University, Busan, Korea
1 Corresponding Author (sasa@maritime.kobe-u.ac.jp)

Abstract:
In recent years, the number of waiting ships in offshore anchorage has increased owing to several reasons, such as the port lockdown and increased cargo volumes in maritime transportations. Moreover, port terminals have ordered ships to stay outside the harbor to prevent mooring accidents when rough waves are forecasted. Anchored ships have been exposed to dangers owing to dragging anchors under rough sea conditions, especially those facing the open seas. In this study, we perform a numerical simulation of anchored ship motions to reproduce the dragging anchor. Additionally, we further evaluated the anchored ship motions based on underestimated wave conditions. Lastly, we constructed a novel risk assessment technique for anchored ships to assess the stranding risk, damage to marine structures, and risk of collision. The stranding risk was evaluated based on the relationship between the vertical displacement and Under Keel Clearance (UKC). Damaging risk can be identified from the information of harbor charts. The risk of collision was quantitatively assessed considering the main influential factors such as Closest Point of Approach (CPA), and the Ship Domain Overlapping Index (SDOI). Results showed that the proposed methodology can contribute to port safety and ship operation in terms of optimal ship routing.

Keywords:
Dragging anchor; Offshore Anchorage; Weather forecasting; Anchored ship motions; Optimal ship routing

1. Introduction

Maritime cargo is estimated to reach approximately 15 billion tons by 2050 (Qinetiq et al., 2013), which indicates that maritime transportation will dominate the world of transportation in the future (Corbett et al., 2010; Ducruet, 2020). However, several factors, such as the optimal ship routing to ensure safety, environmental issues, and energy savings by the Energy Efficiency Design Index (EEDI) enforcement in 2012, could affect safe and efficient transportation. Many related studies have been conducted to minimize gas emission, fuel consumption, and voyage time by accurately estimating the loss of speed in rough seas, etc. (Plessas et al., 2018; Zhang et al., 2019; Du et al., 2021; Sasa et al., 2021). Lockdown measures adopted by various countries due to the corona virus (COVID-19) pandemic caused difficulties and complications for global trade regarding maritime transportation (UNCTAD, 2020). According to CNN (2021) and The New York Times (2021), many ships (around 100 ships) had to stay in offshore harbors for 7-10 days on average due to the increase in maritime transport and the decrease in the number of port workers, which lead to congestion in offshore anchorage. Furthermore, operational issues when ships stay in ports or offshore harbors were also affected. Between 1990-2000, many studies were conducted on moored ship motions to analyze mooring accidents such as the breakage of mooring lines, fenders, quay walls, and ship hulls, caused by long-period waves around 1–3 min (Van der Molen et al., 2006; Figuero et al., 2019). Although it is recommended to enforce mooring facilities in ports to reduce ship motions, very few practice it owing to financial concerns. Therefore, a weather forecasting service was introduced in some ports such as VLCC, LNG, and coal terminals as an alternative countermeasure. In these terminals, the berthing schedules are determined depending on the forecasting systems. The Ministry of Land, Infrastructure, Transport and Tourism, Japan (MLIT, 2009) recommended operation standards for significant wave heights of 0.3–0.5 m inside the harbor and 0.1–0.2 m for long-period waves. Berthing schedules are sometimes adjusted to avoid accidents based on the forecasting system and operational standards. Therefore, ships are ordered to wait at the offshore harbor if rough weather is forecasted (Sasa et al., 2018 and 2019; Lee et al., 2021). However, the safety of anchored ships under severe weather has not been considered. Ventikos et al. (2015) and EMSA (2020) reported that approximately 50-70% of ship accidents occur in port or coastal waters. Sugomori (2010) analyzed several accidents caused by anchoring operations and demonstrated the need for increased knowledge on anchoring operations. However, the current optimal ship routing only focuses on the phase of the voyage in oceans. It makes the total evaluation of ship operations insufficient because safety evaluations such as moored or anchored ships are not considered.

From these backgrounds, this study is organized as follows. Section 2 presents the related studies and describes the methodology for safety evaluation. Section 3 presents the numerical simulation used to reproduce anchored ship motions and describes the algorithms for the risk of

collision. Section 4 summarizes the results of onboard measurement against the 28,000-DWT class bulk carrier for approximately three years in global sea areas. The period of voyage, offshore anchoring, and stay inside the harbor was obtained from the measured data. It was noted that the ship was not on the voyage for approximately 40% of the operation time. Section 5 presents the simulation results of anchored ship motions for each case and compares them with the measured ship motions. The forecasting error should be considered to evaluate the emergency operation in the worst case scenario. Therefore, the simulation of anchored ship motion was conducted if the wave conditions were assumed as the underestimated results. Section 6 presents the construction of risk assessment for the anchored ship including stranding, damaging, and collision accidents in anchorage. In particular, the risk of collision was evaluated by introducing the relative risk factors with the AIS data. Finally, Section 7 presents the conclusions of this study and subjects for future research.

2. Methodology for safety evaluation of anchored ships

This section describes the methodology to conduct the safety evaluation for anchored ships with related studies. Section 2.1 presents the safety evaluation of anchored ship motions in winds and waves. Section 2.2 summarizes the current accuracy of weather forecasting for winds and waves. In Section 2.3, the risk of collisions is additionally introduced for safety evaluation of anchored ships. Based on these points, the methodologies are presented with the main merits of this study here.

2.1. Safety evaluation of anchored ship motions

Some studies have evaluated the anchored ship motions to simulate the dragging anchor, which occurs under strong winds during the offshore harbor refuge for typhoons (Inoue, 1981; Kikutani et al., 1983). However, these studies only considered wind forces. Zou et al. (2012) simulated anchored ship motions considering wave forces besides wind forces; however, the dragging anchors under stormy conditions were not analyzed. Sasa and Incecik (2012) studied the anchored ship motions for a stranded accident offshore harbor facing the Pacific Ocean during the offshore harbor refuge from a big typhoon. The ship stranded after it had drifted into the coast with the dragging anchor of long distances. Additionally, the dynamic model of anchor chain forces and the lumped mass method were introduced to accurately evaluate the mooring forces. Wave forces are considered as the dominant factor in causing ships to be stranded, given that stranding occurs due to vertical motions, and the dragging anchor, other than wind forces, can occur due to long periods of drift forces in irregular sea. The anchored ship motions are compared in each combination of external forces, such as wind forces, linear and non-linear wave forces in time domain motion analysis. It was observed that stranding accidents can occur due to combined

external forces among wind forces, and linear and non-linear wave forces. However, these studies are not widely applied to the safety analysis of ships in coastal sea areas, indicating that the emergency operation still depends on the intuition of ship masters (Sharpey-Schafer, 1954; Zhang and Zhao, 2013; Lu and Bai, 2015). As a result, the accuracy of weather forecasting and knowledge of anchored ship motions becomes inevitable in handling dangerous situations. Theoretical descriptions of anchored ship motions are shown in 3.1 and 3.2.

2.2. Current accuracy of weather forecasting

Many studies have been conducted on weather forecasting at seas, which have been used to operate ships and ports (Chen et al., 2020; Lee et al., 2021). Weather forecasting is one of the most important tools in all ship operation situations and is the fundamental part of optimal ship routing. Despite the various developments in the weather forecasting technology, it is impossible to be perfectly accurate, that is, some errors still exist (Natskår et al., 2015; Girolamo et al., 2017). Chen and Wang (2020) demonstrated that forecasted results are sometimes significantly underestimated against the measured values, by 1.5–2 times. Considering underestimated weather conditions can be very dangerous for ships; it is crucial to understand its influence on ships quantitatively.

2.3. Safety evaluation for risk of collision

Ship motions with dragging anchor are the key factor for evaluating safety for ships in coastal areas. It is important to reproduce the following points, which are vertical ship motions when stranding in shallow waters, damaging structures under the seabed such as cables or pipes by the anchor motion, and collisions with other ships. In the field of maritime transportation, many studies have been conducted on ship domains to analyze the risk of collision (Fujii and Tanaka, 1971; Kearon, 1977; Coldwell, 1983; Pietrzykowski and Uriasz, 2009; Hansen et al., 2013; Wang and Chin, 2016). Im and Luong (2019) proposed Potential Risk Ship Domain (PRSD) to evaluate the potential risk of collision in real time within the Collision Assessment zone. Further, Luong et al. (2021) developed the Marine Traffic Hazard Index (MaTha Index) to represent the dynamic waterway risk. The MaTha Index shows the high-risk collision area of the waterway using the Harbour Traffic Hazard Map. Pietrzykowski and Wielgosz (2021) determined the impact of ship size and speed to ship domain area based on simulation tests. Various risk assessment models of autonomous ships in actual seas have been derived to avoid collision of ships (Tam and Bucknall, 2010; Chai et al., 2017; Liu and Shi, 2020). As mentioned, congestion of ships in the offshore anchorage should be considered given that most collisions occur in coastal areas, especially in the vicinity of anchorage (Yeo et al., 2007; Debnath and Chin, 2016). Burmeister et al. (2014) proposed a collision model for marine risk assessment in offshore anchorages. The model

estimated the risk of collision based on the function of collision frequency and consequence loss.

In most related models, the ship domain have shown as the ellipse shape due to the effect of the forward speed of the ship. However, it is not appropriate to analyze the collision risk of anchored ships with the same ship domain, because the anchored ships have almost zero speed in case of no drift due to dragging anchors. Liu et al. (2020) proposed a model to identify the risk of collision in offshore anchorage using the Automatic Identification System (AIS) database to derive the collision risk index (CRI) between ships in offshore anchorages. To evaluate the index, parameters such as the Distance at Closest Point of Approach, DCPA, Time to Closest Point of Approach, TCPA, and the SDOI were considered the main risk factors. Theoretical descriptions for risk of collision are shown in 3.3.

Fig. 1 illustrates the flowchart of this study. It includes the safety evaluation of anchored ships in offshore harbors, as part of optimal ship routing. Main merits of this study are summarized as:

- Proposing a novel safety evaluation method for anchored ships, thereby enabling discussion on the multiple risk factors such as stranding in shallow waters, damaging with marine structures, and colliding with other ships.
- Predicting the unexpected situation for anchored ships in case of weather forecast failures, which would enhance the safety of offshore anchorage.
- Proposing suitable methods to estimate the collision risk for the anchored ship, which could drift in all directions due to unexpected external forces.

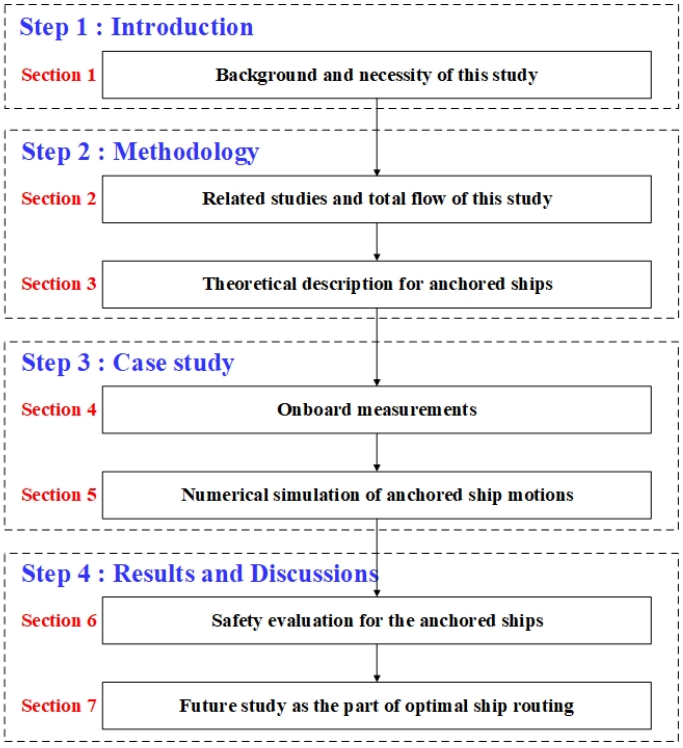

Fig. 1. Flowchart of this study

3. Theoretical description for safety evaluation of anchored ships

This section presents the theoretical descriptions for safety evaluation of anchored ships. First, the numerical simulation for the anchored ships is described in Section 3.1. Next, the lumped mass methods is applied to calculate the anchor chain force in Section 3.2. Finally, in Section 3.3, the collision risk model is illustrated using the various risk factors.

3.1. Numerical simulations for anchored ship motions

Moored ship motions are usually analyzed as the time domain. It is already shown that the time domain model can accurately reproduce measured moored ship motions in the harbor (Kubo and Sakakibara, 1999; Shiraishi et al., 1999). Furthermore, the numerical simulation of anchored ship motions was performed for a ship with a dragging anchor to reproduce the stranded accident offshore harbor in Japan by considering the linear and non-linear wave exciting forces, as well as the dynamic chain force (Sasa and Incecik, 2012). The dragging anchor and strand accident were qualitatively computed if the non-linear wave and dynamic chain forces were considered. For verification, we compared the measured ship motions with the simulated results. Ship motions can be obtained as (Cummins, 1962):

$$\sum_{i=1}^{6}\left(M_{ij}+m_{ij}(\infty)\right)\ddot{X}_j(t)+\sum_{i=1}^{6}\int_{-\infty}^{t}L_{ij}(t-\tau)\dot{X}_j(\tau)d\tau+\sum_{i=1}^{6}\left(C_{ij}+K_{ij}\right)X_j(t) = FWV(t)+FSD(t)+FWD(t)\ (i,j=1,2,\cdots,6) \quad , \tag{1}$$

where M is the mass matrix (including the moment of inertia) of the ship, $m(\infty)$ is the constant added mass, $L(t)$ is the memory effect function, C is the restoring force matrix, K is the mooring force matrix, and X is the displacement vector of ship motions. Subscripts i and j indicate the mode of ship motions. $FWV(t)$ and $FSD(t)$ are the linear and non-linear wave exciting forces, respectively, and $FWD(t)$ is the wind force. $L(t)$ and $m(\infty)$ can be expressed as:

$$L_{ij}(t)=\frac{2}{\pi}\int_0^{\infty}q_{ij}(\omega)\cos\omega t\,d\omega\,, \tag{2}$$

$$m_{ij}(\infty)=p_{ij}(\omega)+\frac{1}{\omega}\int_0^{\infty}L_{ij}(t)\sin\omega t\,dt\,, \tag{3}$$

where $p(\omega)$ and $q(\omega)$ are the added mass and damping coefficient at the angular frequency ω, respectively. Wave exciting forces were computed from the directional wave spectrum in each wave frequency and direction. The non-linear wave forces were obtained using the perturbation

deployment method for each frequency of difference (Bowers, 1989). The wind forces were computed from the irregular wind history, which is the approximated Davenport spectrum. For the frequency analysis, the hydrodynamic and wave exciting forces were computed using the three-dimension Green function method (John, 1950).

3.2. Determining the anchor chain force using the lumped mass method

The anchor chain force was simulated using the lumped mass method, a dynamic analysis model (Walton and Polachek, 1960; Nakajima et al., 1982) that can be applied to situations wherein the anchor chain is not a straight line, including slack condition. Fig. 2 shows the geometrical relationships of the forces around the *j*-th node of anchor chain.

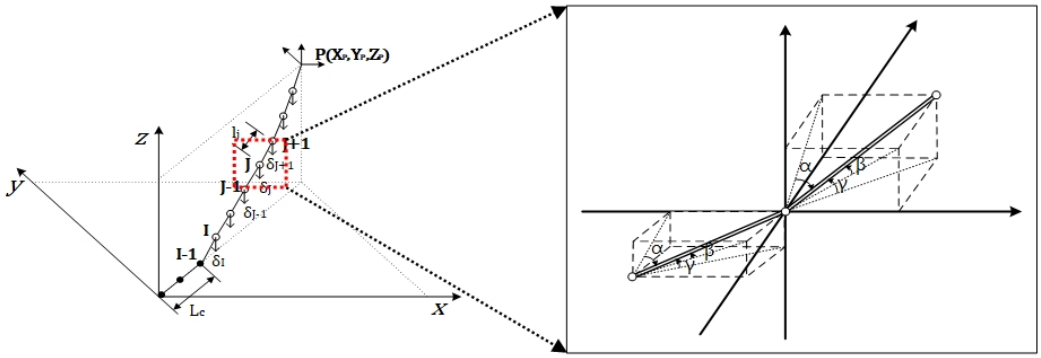

Fig. 2. Discrete representation of the anchor chain and its geometrical relationships

Equations pertaining to the motion around the *j*-th mass point can be expressed as:

$$FX_j = T_j \sin\alpha_j - T_{j-1} \sin\alpha_{j-1} + fx_j \ (j = 2{\sim}N+1) \ , \tag{4}$$

$$FY_j = T_j \sin\beta_j - T_{j-1} \sin\beta_{j-1} + fy_j \ (j = 2{\sim}N+1) \ , \tag{5}$$

$$FZ_j = T_j \sin\gamma_j - T_{j-1} \sin\gamma_{j-1} + fz_j - \delta_j \ (j = 2{\sim}N+1) \ , \tag{6}$$

where FX_j, FY_j, and FZ_j are the total forces in the *x*, *y*, and *z* directions at the *j*-th mass point, respectively, T_j is the tension at the *j*-th math point, and α, β, and γ are the angles between the *j*-th and *j*+1-th mass points. fx_j, fy_j, and fz_j are the drag forces in the *x*, *y*, and *z* directions at the *j*-th mass point, respectively, and δ_j is the weight in the water at the *j*-th mass point. The detail of numerical simulation can be referred to in Sasa and Incecik (2012). The dragging anchor occurs when the anchor chain forces exceed the holding power of the anchor, expressed as the equation of anchor motion:

$$(M_A + m_A)\ddot{X}(t) + D_A\dot{X}_A(t) = T_C(t) - T_{HP}(t) \quad , \tag{7}$$

where T_C, T_{HP}, M_A, m_A, and D_A are the anchor chain force, holding power, mass, added mass, and frictional coefficient of the anchor, respectively. Here, m_A is defined from an empirical model (Ura and Toshim, 1980). The holding power of the anchor can be expressed as:

$$T_{HP}(t) = w_A\lambda_A + w_C\lambda_C L_C \quad , \tag{8}$$

where w_A and w_C are the weights of the anchor and anchor chain per length, respectively. λ_A and λ_C are the drag coefficient of the anchor and anchor chain, respectively. The value of λ_A, which is 10.0 for mud and 7.0 for sand, depends on the seabed conditions. If the dragging distance exceeds 2 times the anchor chain length, λ_A decreases to 2.0.

3.3. Collision risk index for the anchored ship

Many studies have used the concept of the Closest Point of Approaching (CPA), which is the closest point between the underway ship and anchored ship, to calculate and analyze the risk of collision among ships. Fig. 3 illustrates the definition of CPA. The Distance at Closest Point of Approach (DCPA) indicates the closest distance between two ships, when the target ship arrived at the CPA in terms of spatial aspect. The Time to Closest Point of Approach (TCPA) indicates the time taken by a ship to reach the CPA, and represents the risk of collision in the temporal aspect. Related studies reported that the two factors account for nearly 80% of all factors that influence the risk of collision (Zhao et al., 2016; Liu et al., 2019). $DCPA$ and $TCPA$ can be calculated based on the relative distance and bearing between two ships, and the speed of underway ship as:

$$DCPA = Dist \times \sin C_{rbt} \quad , \tag{9}$$

$$TCPA = \frac{Dist}{v_t} \times \cos C_{rbt} \quad , \tag{10}$$

where $Dist$ and C_{rbt} are the relative distance and bearing between ships, respectively. v_t is the speed of the target ship. The relative distance and bearing can be estimated based on the position, bearing, and speed of the ship.

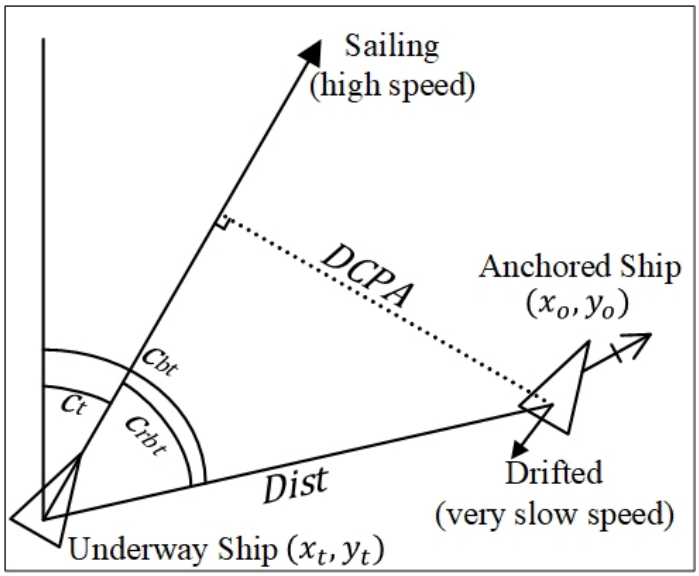

Fig. 3. Illustration of CPA between two ships

$DCPA$ and $TCPA$ can represent the risk of collision between two ships. However, the real-time distance and bearing were not sufficiently included from the concept of CPA. The ship domain has been widely used and developed to examine the collision risk for maritime traffic (Fujii and Tanaka, 1971; Kearon, 1977; Coldwell, 1983; Pietrzykowski and Uriasz, 2009; Hansen et al., 2013; Wang and Chin, 2016). Im and Luong (2019) compared the ship domains of several studies and proposed the PRSD model by calculating the Potential Collision Risk (PCR). However, the ship domains have been considered only for the underway ships, and the anchored ships with low speeds have not been considered. In this study, the ship domain of the underway ships with the forward speed was considered as an ellipse shape with a distance of 1.35 nm in the forward direction, and 0.64 nm in the port, starboard, and afterward directions; further, the ship domain for the anchored ship was considered as the circle shape with the distance of 0.64 nm, as shown in Fig 4.

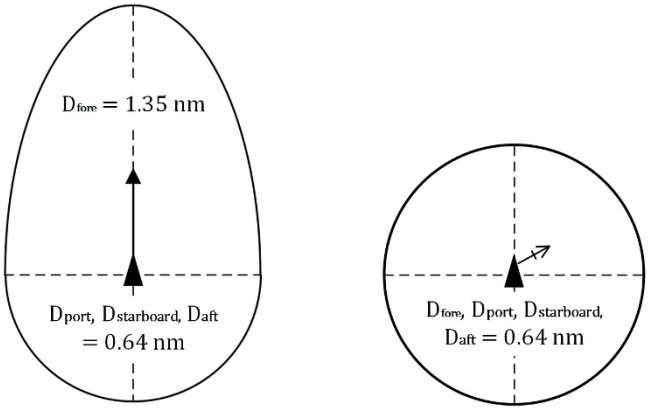

(a) Ship domain for underway ship (PRSD model by Im and Luong, 2019)

(b) Ship domain for anchored ship

Fig. 4. Applying ship domain for underway ships and anchored ships

Im and Luong (2019) introduced the PCR index to reflect the potential collision risk as the combination of non-dimensional $DCPA$ and $TCPA$. The non-dimensional of $DCPA$ and $TCPA$ were obtained as follows.

$$DCPA' = \frac{Dist \times \sin C_{rbt}}{LOA} = \frac{DCPA}{LOA} \quad , \tag{11}$$

$$TCPA' = \frac{Dist \times \cos C_{rbt}}{LOA \times v_t} = \frac{TCPA}{LOA} \quad , \tag{12}$$

where LOA is the ship length overall. The risk diameter R based on the model of Kearon (1977) and the PCR index of Im and Luong (2019) were calculated as follows.

$$R = \sqrt{\lambda DCPA'^2 + TCPA'^2} \quad , \tag{13}$$

$$PCR = e^{-\frac{R^2}{2\sigma^2}} \quad , \tag{14}$$

where λ and σ are the lateral and longitudinal influence parameter. The value of PCR indicated the risk of collision in range 0 to 1, indicating that the risk of collision increased as this value increased.

It was possible to confirm the risk of collision by determining whether these ship domains overlapped or not (see Fig. 5). If the ship domains overlapped, there may be risk of collision. However, it was necessary to express the risk of collision as the quantitative values based on the overlaps.

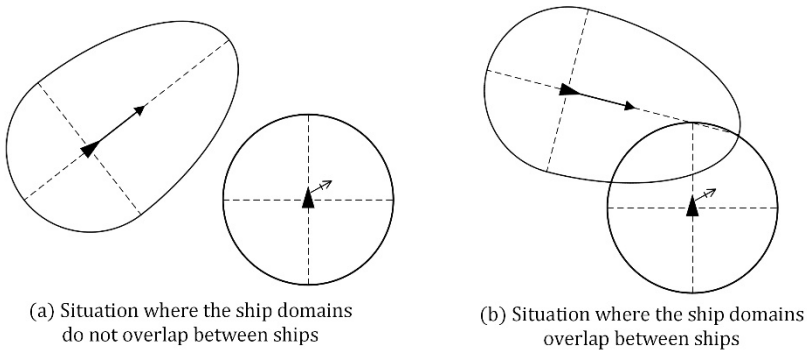

Fig. 5. Situation where two ship domains overlap

To include the relative distance and direction between ships, the SDOI, was introduced for the risk of collision (Liu et al., 2019). The value of $SDOI$ could be obtained by comparing the relative distance of the ships with the safety domain. As the value of $SDOI$ decreased, the risk of collision increased considering the distance of the ship was smaller than that of the ship domain. $SDOI$ between two ships was given as:

$$SDOI = \frac{\sqrt{(x_o - x_t)^2 + (y_o - y_t)^2}}{R_o + R_t} \quad , \tag{15}$$

where R_o and R_t were the radius of the ship domains of the own and target ships, respectively. For the size of the ship domain, different ship domains were applied depending on whether the ship was an underway ship or an anchored ship (see Fig. 4).

It is necessary to quantitatively express the risk of collision using $DCPA$, $TCPA$, and $SDOI$ between ships. In previous studies, a negative exponential function was used to express the relationship between three collision factors and collision risk. The CRI between ships can be obtained as:

$$CRI_{DCPA} = \alpha_D \exp(\beta_D \times DCPA) \quad , \tag{16}$$

$$CRI_{TCPA} = \alpha_T \exp(\beta_T \times TCPA) \quad , \tag{17}$$

$$CRI_{SDOI} = \alpha_S \exp(\beta_S \times SDOI) \quad , \tag{18}$$

where CRI_{DCPA}, CRI_{TCPA}, and CRI_{SDOI} are the CRI of $DCPA$, $TCPA$, and $SDOI$, respectively. α_D, β_D, α_T, β_T, α_S, and β_S are the coefficients for the CRI of $DCPA$, $TCPA$, and $SDOI$ (Zhen et al., 2017). The total CRI of two ships can be identified by combining of collision risk of $DCPA$, $TCPA$, and $SDOI$ linearly, as follows:

$$CRI_{Total} = w_D CRI_{DCPA} + w_T CRI_{TCPA} + w_S CRI_{SDOI} \quad , \tag{19}$$

where w_D, w_T, and w_S are the weight coefficients of each factor. The sum of w_D, w_T, and w_S is 1 and can be preset depending on the traffic situation or the characteristics of the waterway.

4. Case study : Onboard measurements

In this section, the overview of the onboard measurement systems is presented, including the analysis of the total ratio of operation phase for the target ship in Section 4.1. The information on the three case studies is introduced which are staying in offshore anchorage under the rough seas, in Section 4.2.

4.1. Onboard measurements

In this study, we conducted onboard measurements using the 28,000-DWT class bulk carrier, which transported general cargo through a tramper, irregular route. Table 1 summarizes the main dimensions of the bulk carrier. Various parameters pertaining to the performance of the ship operation were monitored by the onboard measurement system, which comprises the motion sensor and the nautical instrument, including the navigation and engine information. The main information of the nautical instrument is the voyage parameters (ship position, ship speed, ship heading, course, and rudder angle), weather data (wind direction and speed), and the engine performance data (engine revolutions, engine power, shaft thrust, and fuel consumption), recorded at 1 s intervals. The motion sensor comprises the inertial measurement unit (NAV440), which measures the rotation angles (roll, pitch, and yaw), rotation angular velocity, and the acceleration along the horizontal and vertical axes, recorded at 0.1 s intervals. This study mainly analyzed the ship position and heading for the anchored ship motions. While the onboard measurement has been continued from 2010 to 2016, the measured data was unavailable for 2011–2012 and 2014–2015 owing to mechanical troubles in the PC drives and electric units.

Table 1 Dimensions of the 28,000-DWT-class bulk carrier

Length between perpendiculars	160.4 m
Breadth	27.2 m
Draft (full loaded/ballasted)	9.82 m / 4.54 m

Several studies have demonstrated that ships encounter 10-15 rough sea conditions during onboard measurements, and the ship performance and weather conditions were analyzed from various aspects (Lu et al., 2017; Chen et al., 2021; Jing et al., 2021; Sasa et al., 2021). However, these studies only focused on the ship operation under voyage in oceans, and hence, the operational situation when the ship has not been on voyage is not known. The tramper, such as a bulk carrier, tends to stay offshore harbor longer than the liner, such as a container ship. The stay period can be roughly divided into the mooring inside the harbor and the offshore anchoring. While the safe operation of mooring inside the harbor has already been studied (Lee et al., 2021), only a few studies have evaluated offshore anchoring based on ship motions in waves. This study clarifies the ratio of operation periods such as voyage, anchoring, and mooring. Furthermore, to classify the operation, the ship was defined on voyage situation if the speed of the ship was over 1.0 knot. The rest of the time was defined as the stay period. It is necessary to divide into the anchoring and mooring, and the ship's heading is used for this division. If fixed, the ship is defined as mooring, and if varied, the ship is defined as anchoring. Additionally, the position of the ship was checked in port terminals or offshore anchorage. Fig. 6 shows the ratio of the operation period of the ship.

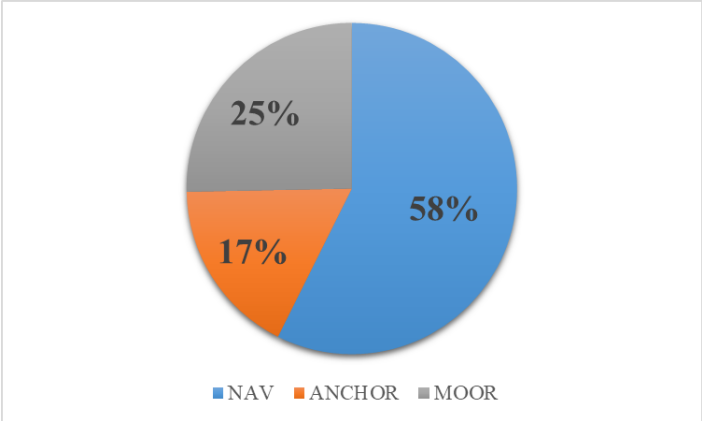

Fig. 6. Total ratio of the operation phase based on the total observation record

As a result, the actual ship status during the voyage was shown as 58% of the total period. Therefore, to complete the optimal ship routing, the ship operation for the remaining 42% of anchoring and mooring conditions must be included. This study focuses on the anchored ship

motions when the ship is affected by rough seas.

4.2. Observation cases of offshore anchoring

During the observation period, the ship sailed and encountered rough seas worldwide, as shown in Fig. 7. The figure also shows the locations of anchorage for these cases. We discuss three cases on large anchored ship motions offshore harbor in rough sea conditions. The ship had been in offshore anchorage facing the open seas in each case. In Case 1, the ship anchored on the coast of Morocco in North Africa, facing the North Atlantic Ocean, and might have waited in offshore anchorage for 7 days before berthing. Although the reason for waiting is unknown, the sea conditions were supposedly rough at that time. When at the offshore harbor, the wind speed and wave height reached approximately 13 m/s and 3.5 m, respectively. In Case 2, the ship stayed in offshore anchorage of Shanghai Port for 2 days, facing the East China Sea. The wind speed had a peak value of approximately 15 m/s, and the significant wave height exceeded 3 m. It is known that larger horizontal motions were measured here, and the ship drifted for nearly 2,500 m. In Case 3, the ship had been anchoring offshore for 6 days on the southwestern coast of Australia, facing the Indian Ocean. During anchoring, the wind speed and wave height reached 18 m/s and 3.5 m, respectively. A low pressure was detected, considering the swirling of wind vector was visible in the distribution of winds, as shown in Section 5.1.

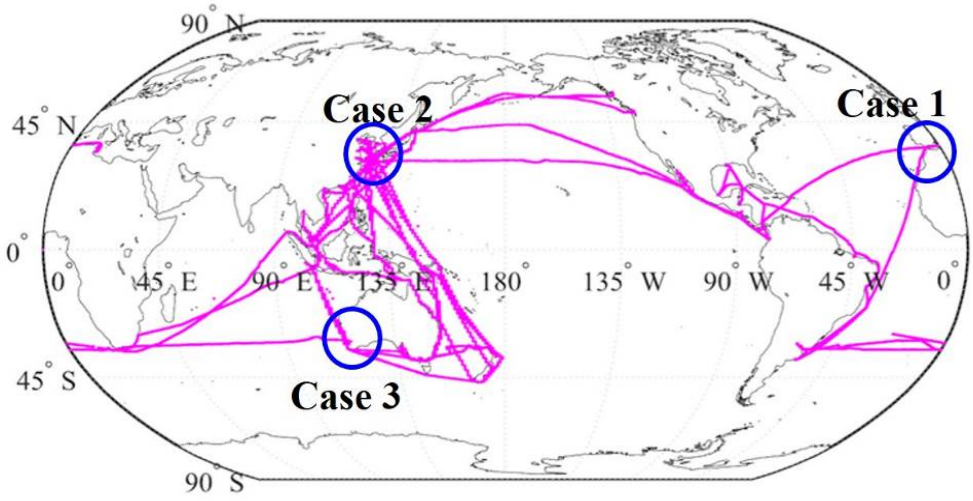

Fig. 7. Ship trajectory during the observation period, and the geographical location for each observation case

5. Case study : Simulation of anchored ship motions

This section discusses the three cases of anchored ship motions based on the measured and simulated results. First, the measured ship motions were reproduced based on the numerical simulations in the previous section to validate the accuracy. Furthermore, we confirm the

reliability of the numerical simulations based on the comparison in each case. Second, the anchored ship motions were simulated assuming the wave height was underestimated. Failed forecasting results can sometimes result in very dangerous situations for ships (Sasa et al., 2014), which could still happen using the current technology of weather forecasting.

5.1. Weather conditions of case studies

Many studies have used the WaveWATCH III (WW3 model; version 4.18) model as the third-generation phase-averaged wave model for the wave hindcasts simulation (Booij and Holthuijsen, 1987; Tolman, 1989 and 2014). Wind input was the most dominant factor in the wave simulation, and there were several kinds of wind input with various spatial and temporal resolutions. Two major databases, the National Centers for Environmental Prediction Final, NCEP-FNL, and the European Center for Medium-range Weather Forecasts Interim Reanalysis, ERA-Interim, were used. Many studies have discussed the validity of wave simulation depending on the wind input sources. Stopa and Cheung (2014) showed that the ERA-Interim wind input generally underestimates the wind speed and wave height. Campos and Guedes Soares (2016) demonstrated that the ERA-Interim wind input resulted in certain underestimation under extreme conditions. Chen et al. (2020) compared the wave simulation results with different wind inputs based on the ship motion calculations. It was found that the NCEP-FNL showed better performance than ERA-Interim for ship routing. Therefore, in this study, the wave simulation was performed using the NCEP-FNL wind input to accurately replicate the rough waves. The WaveWATCH III is a directional spectrum model, and the directional interval is defined as 10°, which covers 36 directions. The range of wave frequencies is set from 0.0345–1.17 Hz and defined by a logarithmic frequency factor of 1.1 for 38 steps. Additionally, to initiate the simulation, a spin-up simulation was performed starting from 1 month ago till the start time in each case. Directional wave spectrum was obtained by solving the equation of motions for defined grids. Distribution of the significant wave height, wave direction, and wave period can be determined from the directional spectrum in each grid. Figs. 8–10 show the distribution of wave height in each case, where the ship position is indicated by the red circle. The red and black arrows represent the wind and wave directions, respectively.

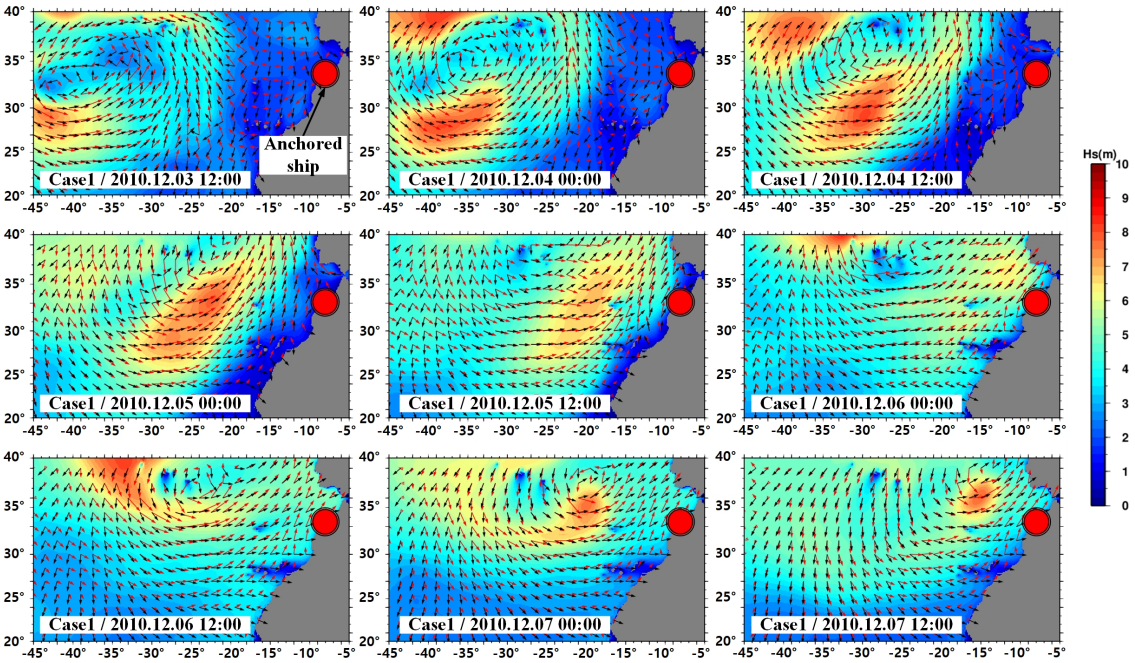

Fig. 8. Case 1: Variations in the weather conditions near Morocco (December 03–07, 2010)

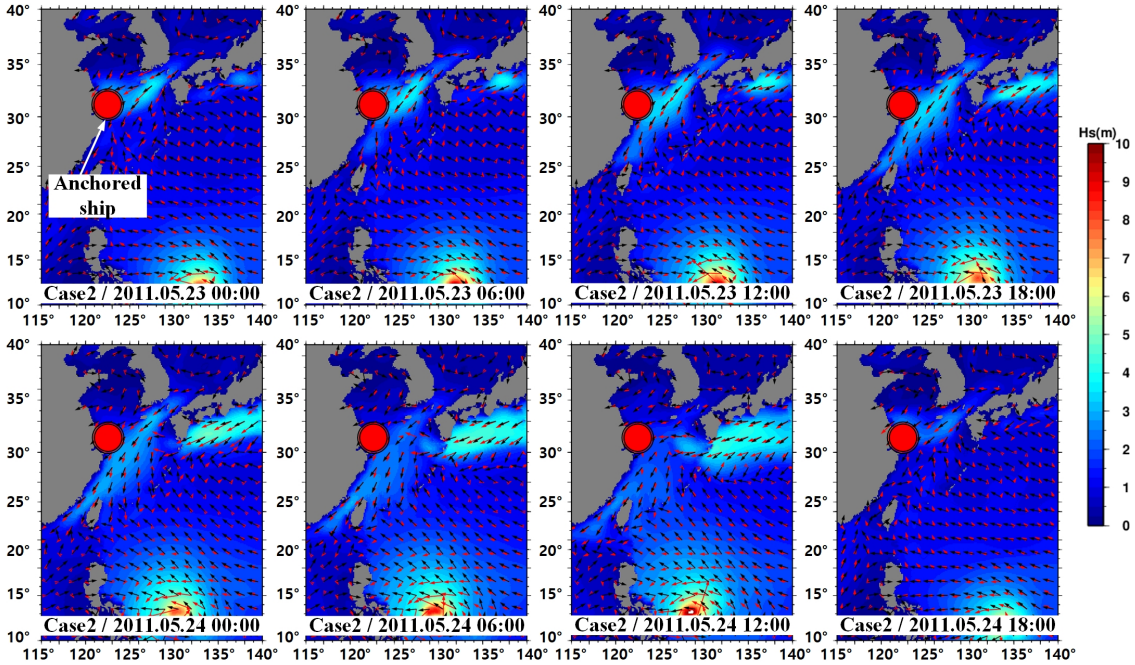

Fig. 9. Case 2: Variations in the weather conditions near China (May 23–24, 2011)

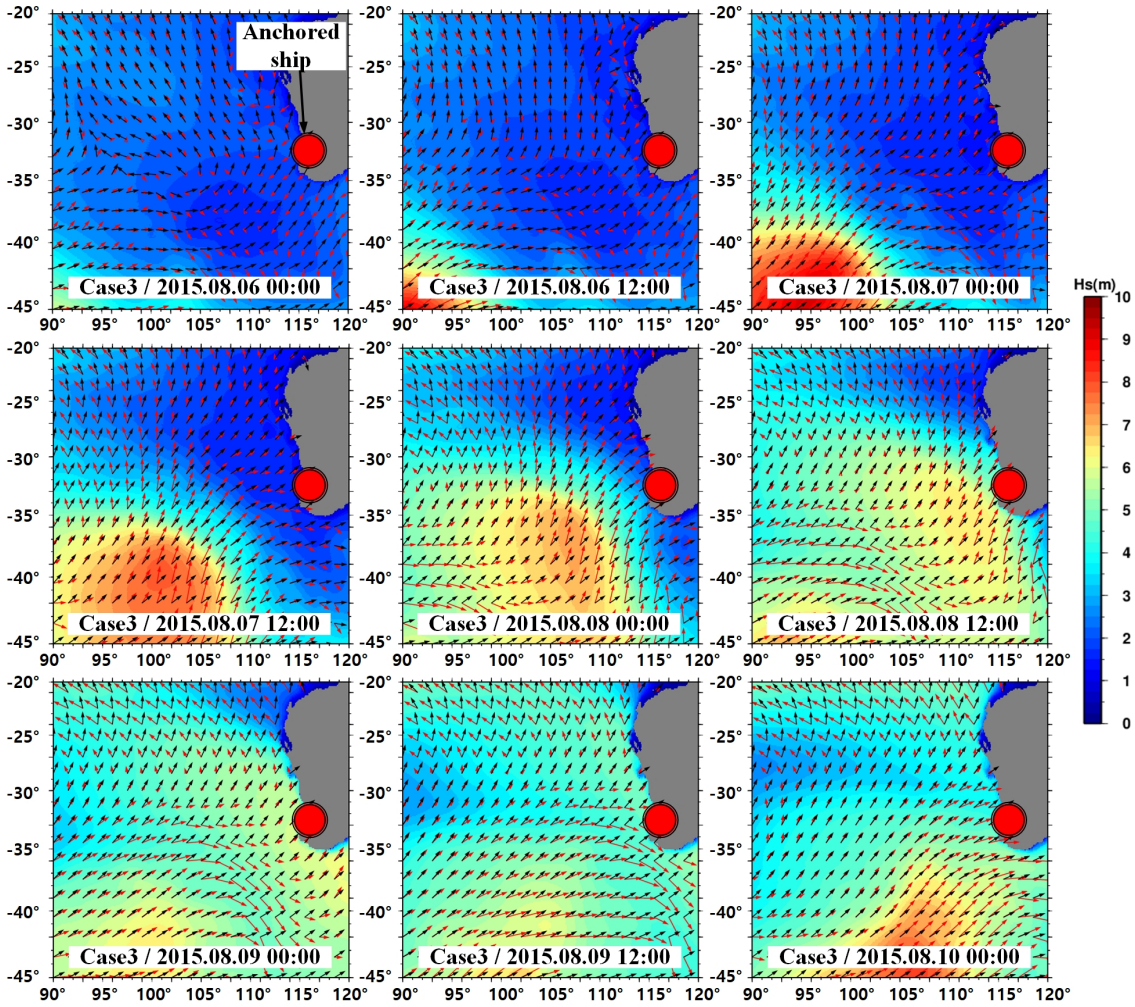

Fig. 10. Case 3: Variations in the weather conditions near Australia (August 06–10, 2015)

The above figures show the existence of strong winds and rough waves in each case. In Case 1, strong winds and waves were observed up to anchorage on the Moroccan coastal area, influenced by a low pressure located approximately 2,000 km west from the anchorage, as shown in Fig. 8. The main wave and wind directions were estimated as Southwest (240-270°) and from South to Southwest (180-240°), respectively, at the maximum wind speed of 12 m/s. Under the weather conditions, the anchored ship was dragged to the northeast.

In Case 2, higher waves exceeding 10 m were observed near the Philippine coast, where a typhoon was located, as shown in Fig. 9. Another high wave was observed offshore the Chinese coast. The wave was generated due to a rainy front from China to Japan instead of the typhoon far from China. The rough sea could threaten the safety of all ships near Shanghai Port, including the anchored ship. Considering the main directions of the waves and winds were almost the same, Northeast (40-60°), the anchored ship might be dragged to the southwest.

In Case 3, higher waves propagated as swells from the Antarctic, whereas the main wave direction was from Southwest to West (240-270°), as shown in Fig. 10. Additionally, the main wind direction was from the Southwest (approximately 240°) at the maximum wind speed of 10 m/s. The wave simulation results showed that the anchored ship may have encountered higher swells and winds, resulting in violent ship motions. Figs. 11–13 compares all three cases for variations in the significant wave height, main wave direction, wind speed, and the wind direction near anchor ship positions.

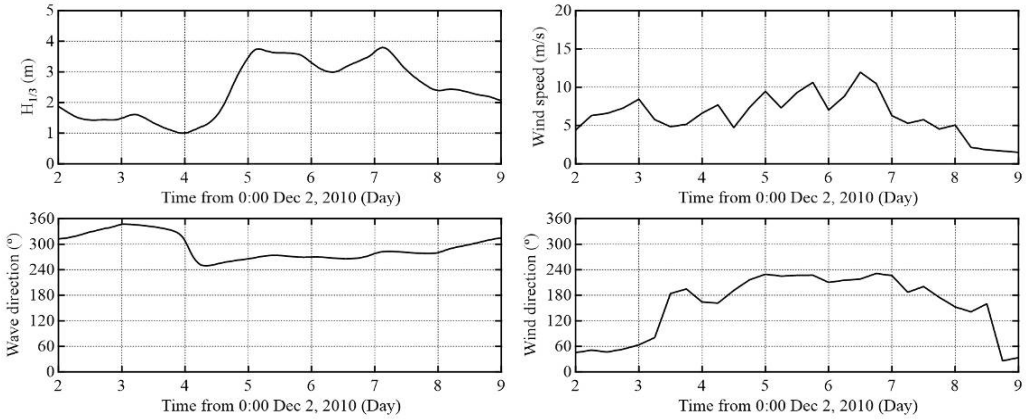

Fig. 11. Case 1: Variation in the weather parameter (December 03–09, 2010)

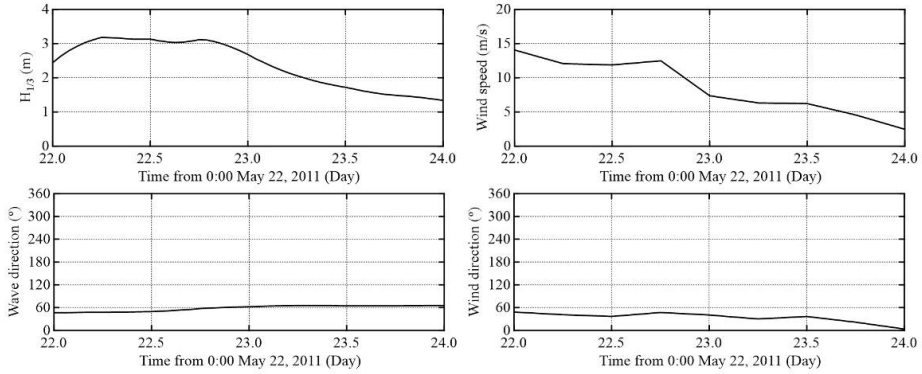

Fig. 12. Case 2: Variation in the weather parameter (May 23–24, 2011)

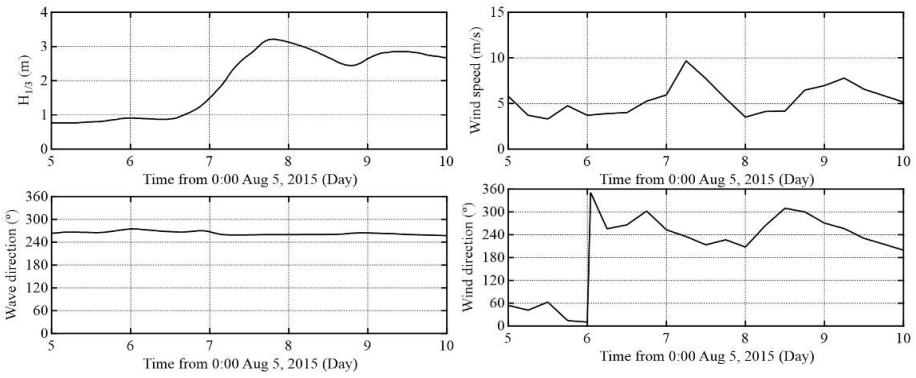

Fig. 13. Case 3: Variation in the weather parameter (August 06–10, 2015)

5.2. Validation of anchored ship motions

We computed the anchored ship motions for the three measured cases to validate the accuracy of the numerical simulations described in Section 3. Environmental conditions of wind waves were numerically simulated using the WaveWATCH III with NCEP-FNL database. Then, anchored ship motions were conducted based on these environmental conditions. The main dimensions of the ship and the anchoring situation are shown in Sections 4.1 and 4.2, respectively. The anchor type used for simulation was AC-14, with a weight of 5.51 tons and anchor chain diameter of 66 mm with the weight per unit length of 0.1045 tons. Table 2 summarizes the simulation period, location, loading conditions of the ship, seabed materials, and the water depth.

Table 2 Loading conditions, seabed material, water depth, and simulation period

No.	Simulation period	Location	Loading condition	Seabed material	Water depth
Case 1	From 12:00 Dec 3 to 04:00 Dec 6, 2010	Jorf Lasfar, Morocco	Ballasted	Gravel and sand	40 m
Case 2	From 7:00 May 23 to 04:00 May 24, 2011	Shanghai, China	Fully loaded	Mud and sand	29 m
Case 3	From 12:00 Aug 6 to 14:00 Aug 10, 2015	Bunbury, Australia	Ballasted	Sand	23 m

The loading condition was ballasted in Cases 1 and 3 and fully loaded in Case 2. The left-hand side figures in Fig. 14 show the simulated results of the ship track on the gravity point, and are compared with the measured results. The right-hand side figures show the analyzed results of the drifted distance with horizontal ship motions from the initial ship position.

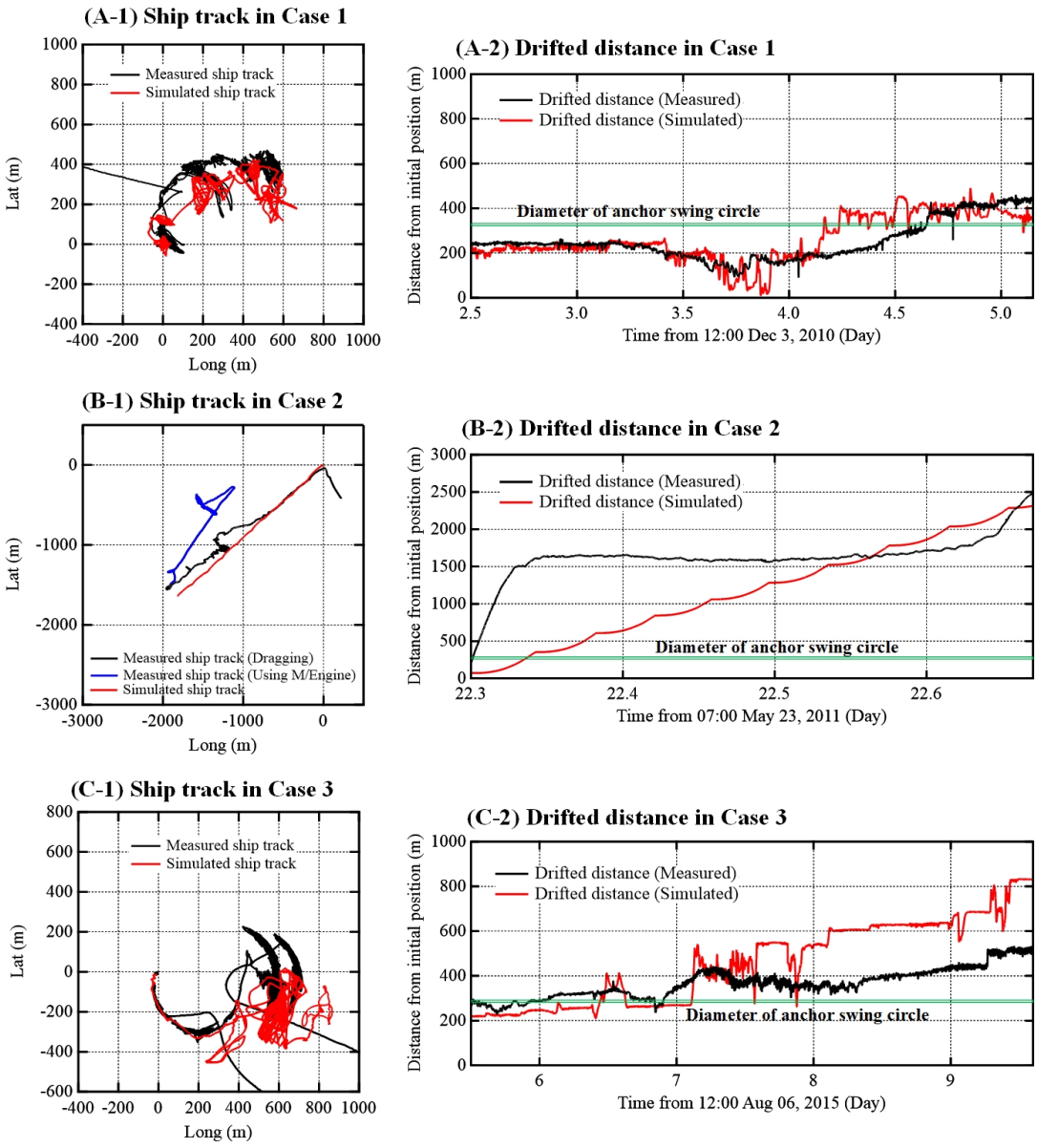

Fig. 14. Comparison of the ship track and the drifted distance from the initial position between simulation (Red) and measurement (Black, blue)

The simulated and measured ship tracks are indicated by the red, black, and blue lines, respectively, in the left-hand side figures in Fig. 14. The origin of ship tracks is defined as the initial position of the anchored ship for each case. The simulated and measured drifted distances from the initial ship position are indicated in red and black lines, respectively, in the right-hand figures. Herein, we can observe that the dragging anchor occurs by comparing the drifted distance and the anchor swing circle. The diameter of the anchor swing circle is similar to the length of the anchor chain (Gao and Makino, 2017), which has been recommended based on the formula

(Length of anchor chain = 4 × water depth + 145 m) for stormy weather (MAIA, 2006). The anchor swing circles are indicated for each case by green lines in the right-hand side figures. We can say that the ship drags her anchor when the drifted distance is greater than the anchor swing circle.

Case 1 shows that the ship drifts approximately 200 m in the initial 2 days, indicating that the ship does not drag her anchor given the drifted distance is less than 305 m of the anchor swing circle (= 4 × 40 + 145). On the last day (5 December 2010), the ship drags her anchor, indicating that the drifted distance was over 400 m. The measured ship track showed that the ship continuously pushed towards the northeast, which coincides with the simulated ship track, as shown in Fig. 14 (A-1). Furthermore, a good agreement was observed between the simulation and measurement results, with final drifted distances of approximately 400 m and 420 m, respectively, as shown in Fig. 14 (A-2).

Unlike the other cases, the anchor swing circle was not visible at all in Case 2, and the ship only drifted for approximately 2,500 m. Therefore, from the analyzed result of measured data, we can assume that the dragging anchor occurred considering the ship did not use the main engine at that time. As the ship drifted near the entrance of fairway, it used the main engine to move back to the original anchoring position, as indicated by the blue line in Fig. 14 (B-1). Before the ship uses the main engine, the simulated ship track follows the measured ship track, which is drifted to the southwest. The simulated and measured total distances from the origin were 2,300 m and 2,500 m, respectively, as shown in Fig. 14 (B-2). However, some major differences were observed between the simulated and measured results. According to the measured data, the dragging anchor occurred dominantly in the initial 1 h. From the total distance of 2,500 m, the main dragging of 1,700 m was observed in the first 1 h, whereas the remaining 800 m was observed in the last one hour. In contrast, the drifted distance of the simulated results showed that the ship continued to drift for 2,500 m. Although the tendency of dragging between the simulation and measurement results was different, the direction and distance of the dragging situation can be reproduced using the simulation model.

During the initial days of Case 3, the measured ship track followed the range of the anchor swing circle, as shown in Fig. 14 (C-1). Furthermore, the drifted distance from the anchor circle coincided with the diameter of the anchor swing circle at that time as shown in Fig. 14 (C-2). On 08 August 2015, the drifted distance was greater than the diameter of the anchor swing circle, indicating that dragging anchor has occurred. At that time, high waves exceeding 3 m propagated along with the ship position, as shown in Figs. 10 and 13. It is obvious that the large horizontal ship motions were influenced by the strong waves. On comparing the measured and simulated ship tracks for Case 3, it was found that the simulation results were overestimated, which was

approximately 800 m and 550 m of the drifted distance in simulation and measurement, respectively.

The simulation model in this study showed errors of approximately 50 m, 200 m, and 250 m in the drifted distance in Cases 1, 2, and 3, respectively, which can be attributed to errors between the simulations and measurements. One of the main reasons is the uncertainty of the wave simulations, which could not accurately replicate the weather condition. Owing to this, errors may have occurred in the anchored ship motions. Although the simulation model of anchored ship motions showed differences, the anchored ship motions were reproduced well by this model and coincided with the direction and tendency of the measured ship tracks. Especially, the model was able to reconstruct the presence of the dragging anchor, and accurately detect the time and direction of the dragging anchor.

5.3. Comparative simulation of the anchored ship motions in case of weather forecasting failures

Several studies on the weather forecast have demonstrated the errors and uncertainties of weather forecasting systems (Girolamo et al., 2017; Chen and Wang, 2020). The uncertainties of weather forecasting can endanger marine operations considering the operations are planned and conducted based on the weather forecasting information to minimize the risk under rough seas. (Natskår et al., 2015). Therefore, it is essential to recognize the uncertainties of weather forecasts for the safety analysis of the ship operation pertaining to optimal ship routing.

To investigate the differences based on the weather forecasting failures, it is necessary to conduct further simulations for the anchored ship motions, with 2–3 times the wave height for more severe weather. Fig. 15 shows the variations in the actual waves and waves that are 2–3 times higher than the significant wave height for each case. “U-1”, “U-2”, and “U-3” represent the significant wave heights for the actual wave condition, 2–3 times of the underestimated wave conditions, indicated by black, blue, and red lines, respectively. For these simulations, the wave forces were only changed based on the significant wave height. The other weather conditions, such as the wave direction, wind speed, and direction were not changed.

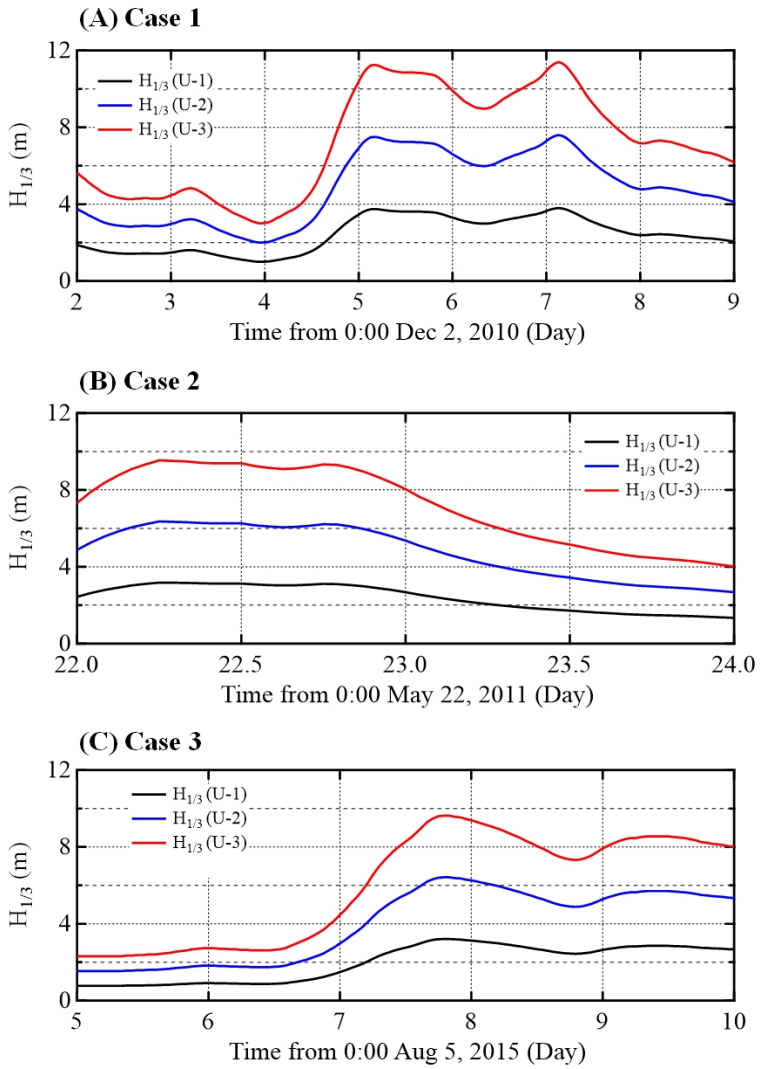

Fig. 15. Variations in the significant wave height of each case

Fig. 16 shows the simulated results of the ship track on the gravity point under different wave conditions. Furthermore, the analyzed results of the drifted distance with horizontal ship motions from the initial ship position are shown in the right-hand side figures of Fig. 16. The simulated results under U-1, U-2, and U-3 conditions are indicated by black, red, and blue lines, respectively. The origin of ship tracks was defined as the initial position of the anchored ship for each case.

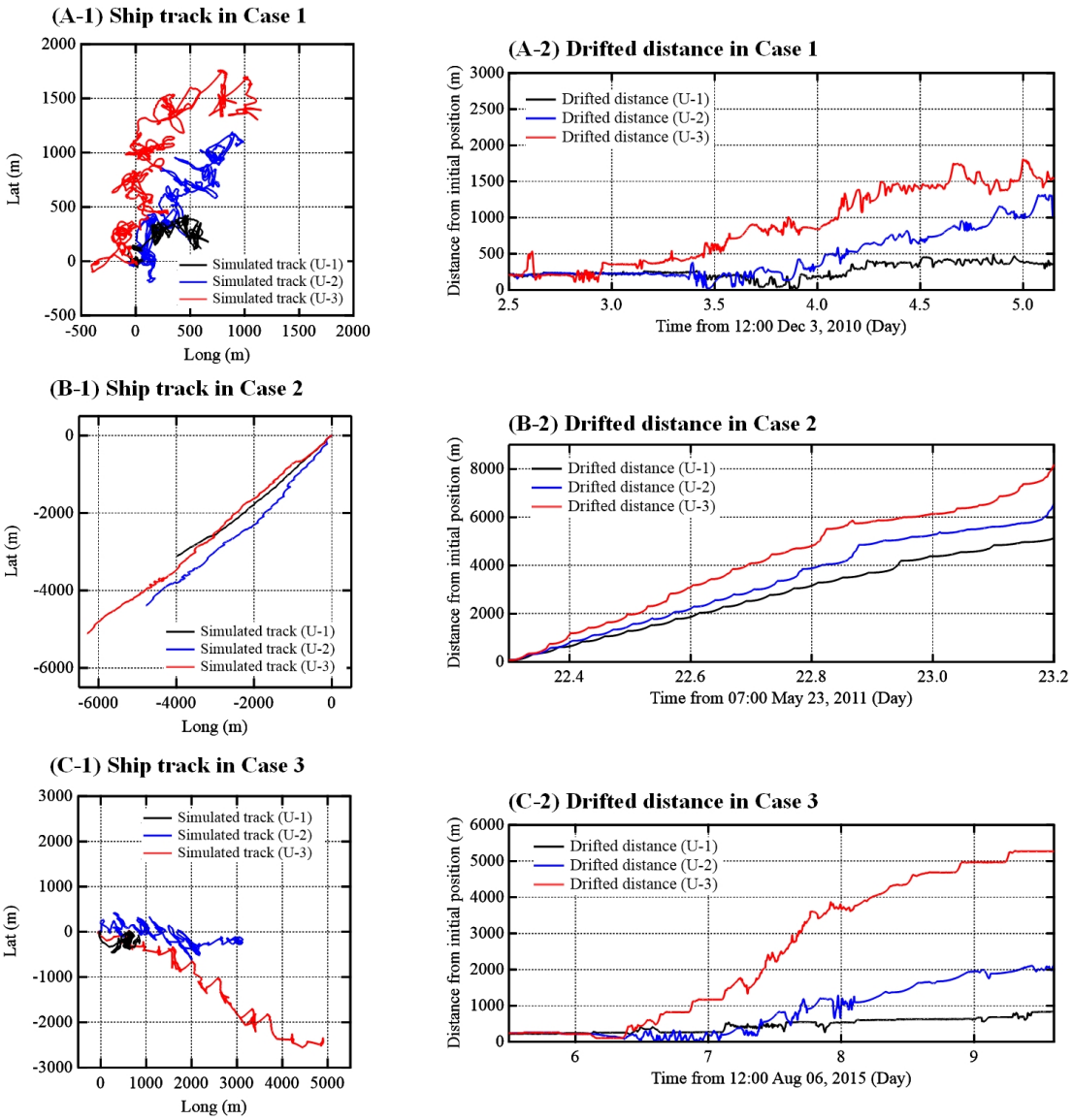

Fig. 16. Comparison of the simulated ship tracks and the drifted distances from the initial position under different wave conditions

In Case 1, the drifted distance from the initial position was less than 500 m under U-1 condition. Larger horizontal ship motions were observed under the more severe waves. The distance reached 1300 m and 1800 m under U-2 and U-3 conditions, respectively, indicating that the wave height significantly influenced the anchored ship motions. The main wave direction was from the southwest (240–270°), and hence, contributed to the horizontal ship motions in the northeast direction.

The measured data of Case 2 showed that the ship used the main engine after drifting for approximately 2,500 m. Herein, the simulations were conducted assuming the ship was

continuously exposed to rough seas without using the main engine. The ship drifted for approximately 5,000 m under U-1 condition, which increased to 6,200 m and 8,000 m under U-2 and U-3 conditions, respectively. If the ship approached the fairway, it might encounter a dangerous situation.

In Case 3, the ship drifted for approximately 800 m under U-1 condition, which increased to 2,000 m and 5,000 m as the height increased under U-2 and U-3 conditions, respectively. It is obvious that the ship motions were not proportional to the wave heights, indicating that the high waves implicated large horizontal ship motions although the anchored ship motions were irregular, non-linear to the wave height. This point needs to be investigated further in future studies.

6. Results and discussions

In this section, the potential risk of the anchored ship was newly evaluated for the entire safety of offshore anchorage. Although anchored ships are usually defined as fixed and immobile structures, the ship can drift for more than a nautical mile in rough seas. Therefore, to construct the risk assessment for the anchored ships, it is necessary to identify the risk in anchorage. Furthermore, the potential risk factors for anchored ships should be identified and analyzed depending on the accident reports and previous studies (Sugomori, 2010; Sasa and Incecik, 2012; Debnath and Chin, 2016; Gao and Makino, 2017). While previous studies only concentrated on stranding, this study presents the novel risk assessment method for anchored ships while including various parameters such as shallow depth, marine structures, and traffic situations, as shown in Fig. 17.

The variables of potential risk can be verified by analyzing the data using the navigational harbor chart for each case in Section 6.1. Furthermore, the historical AIS data, which can sufficiently explain the marine traffic situations, was used to further investigate the risk of collision in Section 6.2.

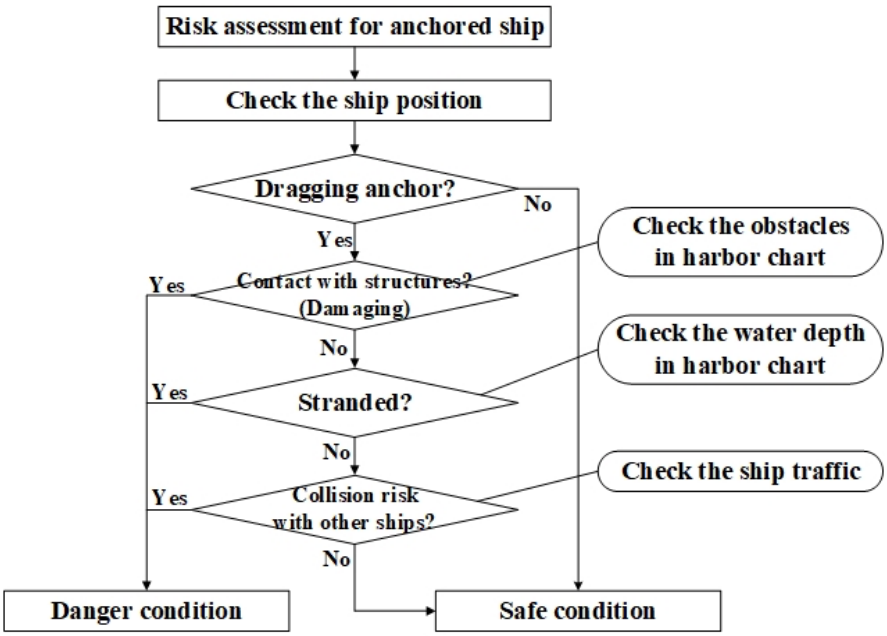

Fig. 17. Flowchart of the novel risk assessment method for anchored ships

6.1. Safety evaluation of the anchored ship by the harbor chart

It is crucial to obtain fundamental information such as water depths and obstacles to identify the accident of damaging marine structures and stranding to shallow water. The fundamental information can be obtained from the harbor charts, as shown in Fig. 18.

Damaging accidents usually occur by contact with the dragged anchors to marine structures installed on the seabed, such as pipelines or cables. Initial anchor positions and drifted ranges from the simulated results are marked for each case in Fig. 18. The black, blue, and red circles indicate the range of simulated ship tracks under U-1, U-2, and U-3 conditions, respectively. Fig. 18 also shows that there are no marine structures around the ship trajectories in all three cases, indicating the relatively low risks of damage to marine structures by the dragging anchor.

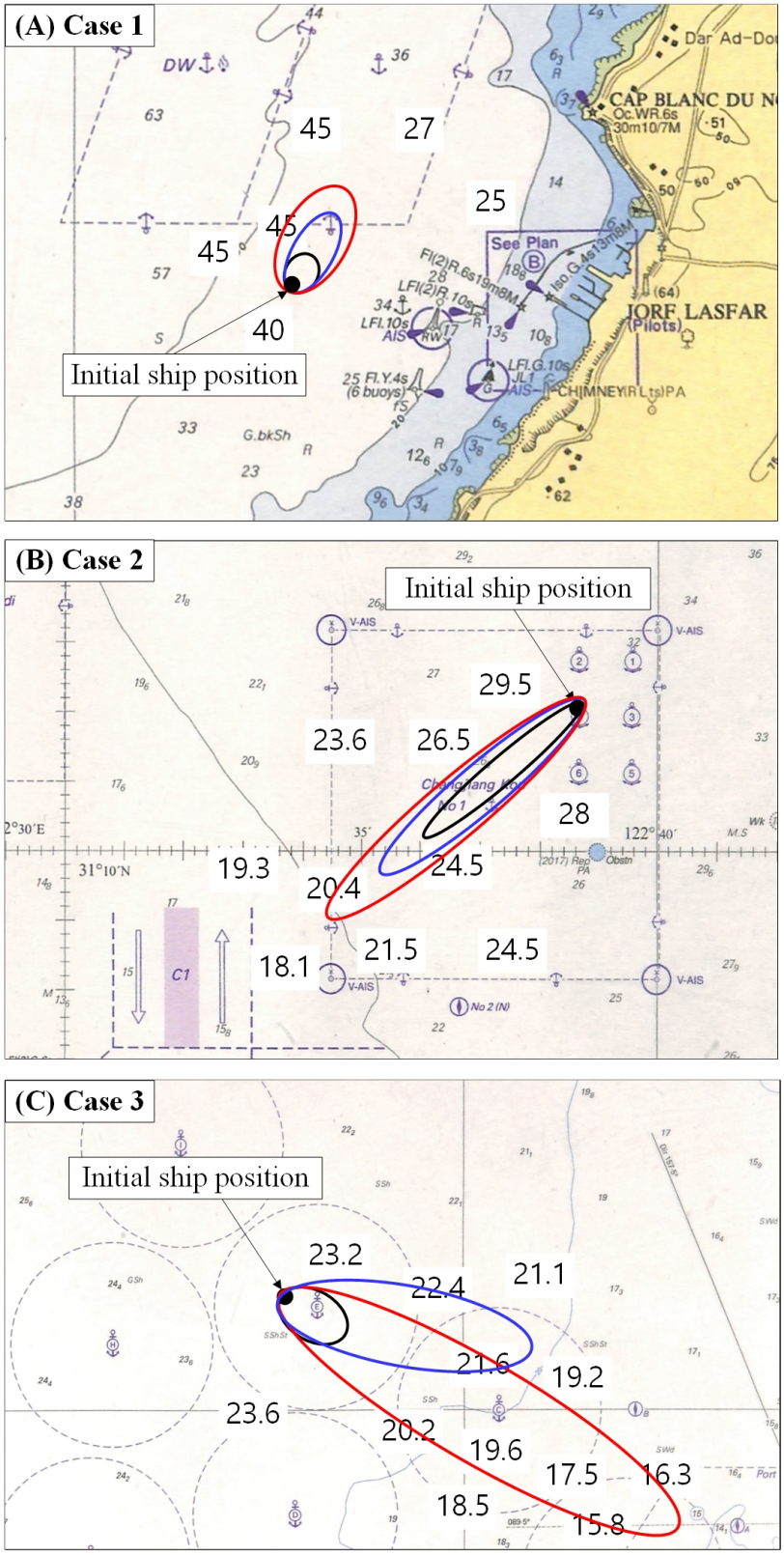

Fig. 18. Harbor chart with the drifted range of the simulated ship tracks for each case

Standing accidents occur owing to the relation between the Under Keel Clearance (UKC) and the vertical displacement due to heave, pitch, and roll motions. The UKC is decided based on the relation between draft and water depth. It is obvious that the minimum water depths are approximately 40 m, 20 m, and 15 m at the farthest drifted position in Cases 1, 2, and 3, respectively, as shown in Fig. 18. To evaluate the stranding accident, the UKC is calculated as (Sasa and Incecik, 2012):

$$UKC(t) = W_M - D - \left(\frac{L}{2} - MG\right)\sin X_4(t) - \frac{B}{2}\sin X_5(t) - X_3(t) \quad , \tag{20}$$

where W_D is the minimum water depth, D, L and B are the draft, length, breadth of the ship, respectively. MG is the distance between the gravity point and midship. $X_3(t)$, $X_4(t)$, and $X_5(t)$ are the vertical ship motions of heave, pitch, and roll, respectively. Fig. 19 shows the calculated results of UKC.

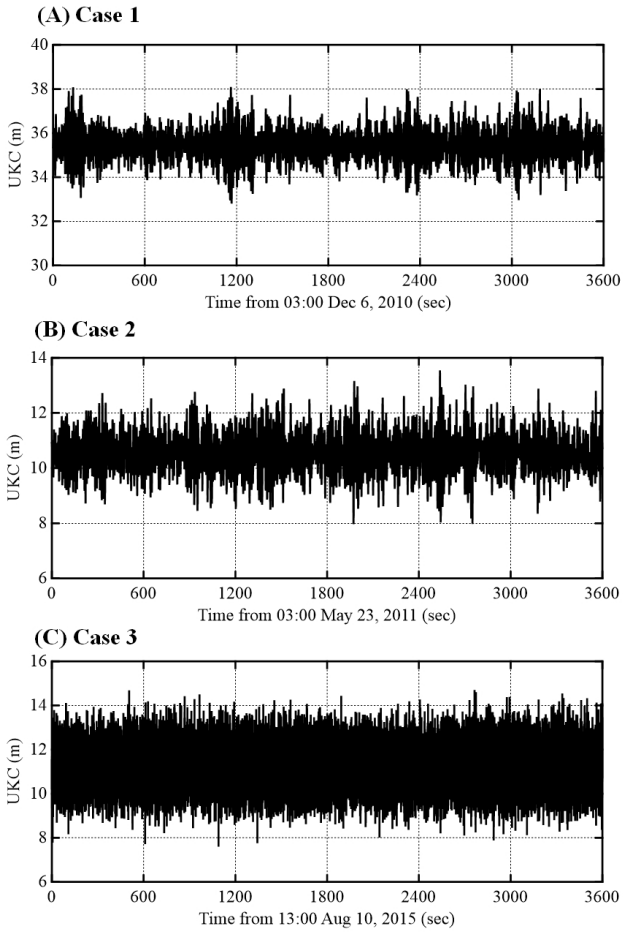

Fig. 19. Calculated under-keel clearance at the minimum water depths for each case

The stranding risk is determined by the UKC. If the UKC value reaches 0, the ship might be stranded by the shallow water. As shown in Fig. 19, the minimum UKC has adequate margins of approximately 32 m, 8 m, and 8 m from the seafloors in Cases 1, 2, and 3, respectively, which indicates that there are relatively low risks of stranding. Although the ship drifts more than a nautical mile, it is obvious that the ship might not be in danger of stranding or damage based on the chart information and UKC calculations.

6.2. Safety evaluation of the anchored ship using AIS data

To further investigate the collision risk of the anchored ship, it is essential to figure out the marine traffic characteristics with the historical AIS data. Although historical AIS data is purchased from the exactEarth Ltd., the amount of dynamic information (position, speed, heading, etc.) is less in Cases 1 (2010) and 2 (2011), making the analysis very difficult. Therefore, only the risk of collision for Case 3 (2015) was evaluated.

The AIS data for Case 3 was analyzed for 3 days from August 7 to 9, 2015, when the rough sea condition prevailed. The safety of the anchored ship was evaluated in the area between 115.50° E to 115.67° E longitude and 33.20° S to 33.32° S latitude. Approximately 13 ships enter or depart the harbor, as shown in Fig. 20.

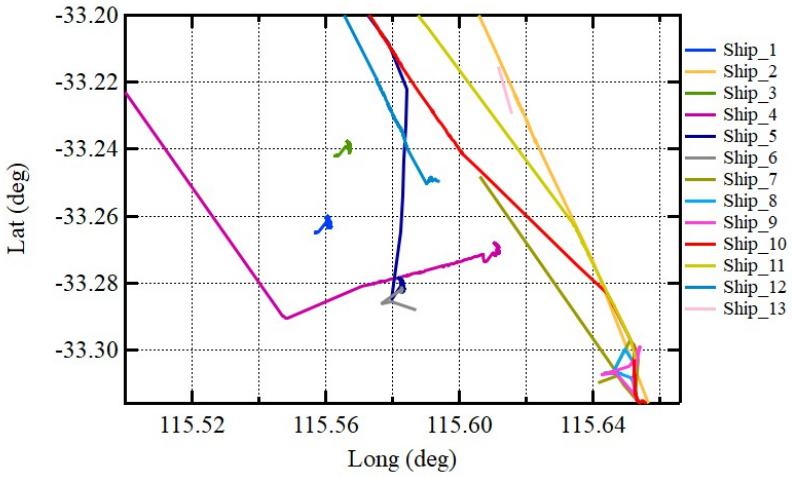

Fig. 20. Historical AIS data for all ships in Case 3 during 07-09 Aug, 2015

In Case 3, 3 ships approached the anchored ship within the distance of 2,500 m, which can cause a higher risk of collision. Trajectories of the 3 ships varied for 3 days, as shown in Fig. 21. “Own ship” represents the bulk carrier that was measured and simulated in the previous section. “Ships (A), (B), and (C)” represent the ships approaching the “Own ship”. Ship (C) drops its anchor after passing the own ship at the distance of 1,425 m and stays for nearly 3 days with little movement. On August 9, ships (A) and (B) approached the own ship at distances of 2,275 m and

1,310 m, respectively. Ship (A) entered the harbor after passing there. Particularly, high collision risk was expected with ship (B), considering ship (B) stayed with an anchor within a nautical mile from the Own ship. Although anchored ships are usually defined as the stationary subjects (Debnath and Chin, 2016; Liu et al., 2020), it is necessary to consider the drifting speed owing to the dragging anchor.

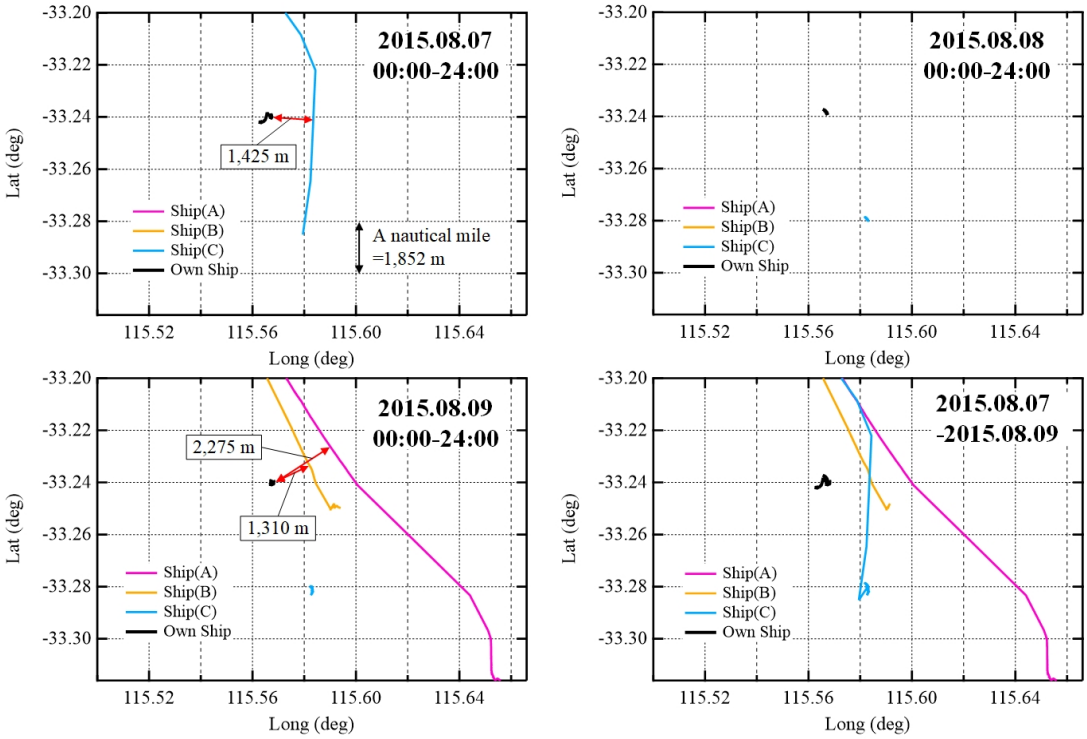

Fig. 21. Relationship with between the own ship and the closest three ships

6.3. Result of collision risk for the anchored ship

The risk of collision was estimated from the simulated results of anchored ship motions. When the weather forecast was underestimated, as shown in Section 4.3, the drifted distance increased from 800 m under U-1 condition to 5,200 m under U-3 condition. Fig. 22 shows the variations in the PCR and CRI of each ship (Ships [A], [B], and [C]) under different wave conditions (U-1, U-2, and U-3 conditions).

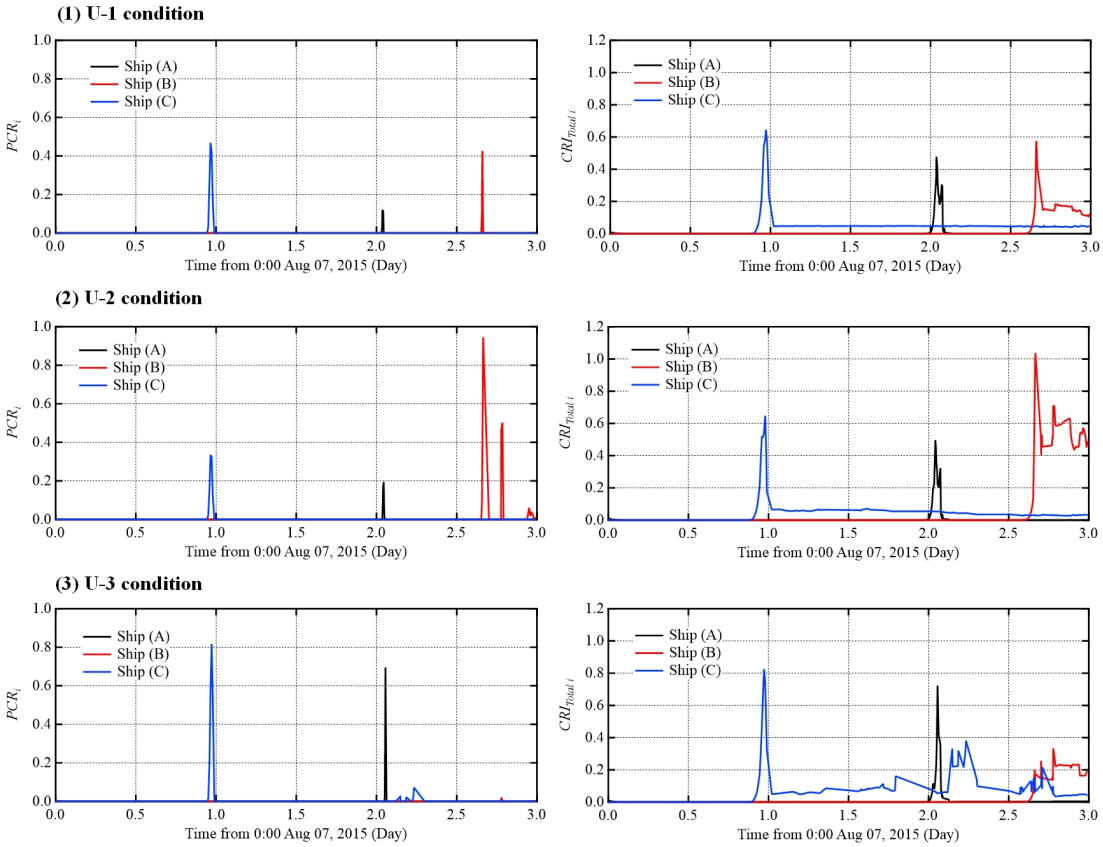

Fig. 22. Results of the total CRI for each ship

The collision risk with ship (C) increased to approximately 1.0 day when it passed the anchored ship at a distance of 1,425 m (0.77 nm). Then, ship (C) dropped the anchor near the own ship (the anchored ship), and the value of PCR and CRI was less than 0.2 after the peak value at approximately 1.0 day. Furthermore, ship (A) passed the own ship at a distance of 2,275 m (1.23 nm) on around 2.1 day. Ship (A) did not stay near the own ship, indicating that the value of PCR and CRI only increased around 2.1 days, and was almost zero for the rest of period. Ship (B) passed the own ship at a distance of 1,310 m (0.71 nm) at around 2.7 days. The collision risk of ship (B) was expected to be higher, especially for the underestimated cases (U2 and U3 conditions), considering the own ship (anchored ship) had drifted for 2,000 m to 5,200 m (1.08 nm to 2.81 nm) owing to the dragging anchor towards ship (B). This increased the value of PCR (from 0.4 to 0.9) and CRI (from 0.6 to 1.1) of ship (B) under U-2 condition. However, the value of PCR decreased to zero and the value of CRI decreased to 0.3 under U-3 condition, irrespective of whether the wave height was three times underestimated. As Fig. 16 (C-1) shows, the drifted distance under U-3 condition was approximately 5,200 m (2.81 nm). Therefore, the own ship (anchored ship) had already passed the area before ship (B) arrived at the anchorage. Fig. 23 shows the comparison of the maximum values of PCR and CRI.

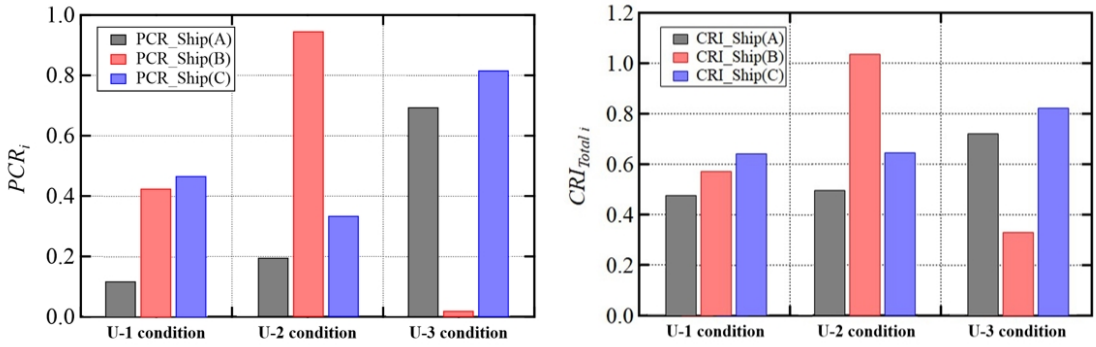

Fig. 23. Comparing each ship's maximum PCR and CRI values

The results of PCR and CRI showed that the risk of collisions increased as the weather worsened, with a few exceptions. The collision risk with ships (A) and (C) increased as the weather conditions worsened, especially in U-3 condition (three times the wave heights). This indicated that the drift due to dragging anchor could increase the risk of collision, even in the anchoring situation. However, there was a difference in the results of collision risk with ship (B) in U-3 condition. The value of PCR with ship (B) was almost 0.0, while the value of CRI was approximately 0.3, showing the risk of collision. As mentioned, the own ship had already passed the route of ship (B) in U-3 condition, which reduced the risk of collision in terms of DCPA and TCPA. The calculation of PCR could not reflect the relative distance between ships because it was based on DCPA and TCPA. Since the anchored ship could drift in all directions due to unexpected external forces, the CRI method including the relative distance and bearing was more reliable than the PCR method in case of offshore anchorage.

Results of collision risk showed that anchored ship motions were inevitable for accurately evaluating the collision risk in offshore anchorage. However, there are very few studies on the collision risk considering anchored ship motions. Furthermore, the safety evaluation of offshore harbor is essential, besides the safety in voyage and harbors, as part of the optimal ship routing.

7. Conclusions

Optimal ship routing is the key foundation to the safety of ship operations, including sailing in the ocean, mooring inside the port, and anchoring outside the harbor. However, very few studies have considered the anchoring status in optimal ship routing. Furthermore, it is necessary to develop safety measures for anchored ships in underestimated weather conditions, given that anchored ships have been exposed to accident risks such as stranding, and collision with other ships under rough seas. Stranding can be evaluated by the UKC based on the water depth, the draft of the ship, and the vertical ship motions. Furthermore, the risk of collision should be considered simultaneously. The anchored ship should be treated as a movable object with a

dragging anchor. In this study, we simulated anchored ship motions to validate the results with the onboard measurement results. Furthermore, additional simulations were conducted under underestimated wave conditions. The risk of collision was evaluated using the AIS data and anchored ship motions. The main conclusions of this are as follows.

(1) For the simulation of anchored ship motions, the directional wave spectrum can be given as the computation of the WW III model with NCEP-FNL wind source. The anchored ship motions can be reproduced using the directional wave spectrum and showed good agreement with the onboard measurement results. It quantitatively shows how the anchored ship motions and drifted distance increase with underestimated wave conditions.

(2) A novel risk assessment for anchored ships were constructed, which included the risk of stranding in shallow waters, damaging structures on the seabed, and the risk of collision with neighboring ships. The stranding was evaluated based on the relation between the estimated UKC owing to the vertical motions and water depth. The damaging accidents were evaluated based on the existence of obstacles near the simulated ship position.

(3) The index for the risk of collision was evaluated based the factors such as the DCPA, TCPA, and SDOI. It was observed that the drifting of the ship strongly influenced the risk of collision. The risk of collision increased simultaneously if the drifted distance increased as the underestimated wave condition worsened. However, the risk of collision decreased for one of the ships near the anchored ship, even if the underestimated wave height was 3 times higher. This indicated that the risk of collision depends on the relationship between time-varying anchored ship motions and the surrounding traffic situation.

(4) Anchored ships should be treated as drifting object when ships drift over the swing circle of anchoring. This should be considered in future studies on collision risk. Furthermore, it is necessary to apply the methodology of this study to other ship types and sea areas to develop optimal ship routing.

However, the proposed risk assessment still had some limitations. Here, the potential risk for the anchored ships was individually evaluated with the three aspects (i.e., stranding, damaging, and colliding). It was necessary to express the total risk index to evaluate the offshore anchorage. Furthermore, the safety evaluation was conducted with the one target ship, applying to the three anchorages. Therefore, it is necessary to include the various type and size of ships and port terminals to standardize the risk level in the future study.

Acknowledgments

The authors wish to extend their gratitude to the Shoei Kisen Kaisha, Ltd. and Imabari Shipbuilding Co., Ltd., for their cooperation in conducting the onboard measurements of the 28,000-DWT bulk carrier from 2010–2016. This study was financially supported by Scientific Research (B) (Project No. 20H02398, 2020–2024, represented by Kenji Sasa) and Fostering Joint International Research (B) (Project No. 18KK0131, 2018–2022, represented by Kenji Sasa) under Grants-in-Aid for Scientific Research, Japan Society for the Promotion of Science.

References:

Booij, N. and Holthuijsen, L. H., 1987. Propagation of ocean waves in discrete spectral wave models. *Journal of Computational Physics*. Vol. 68, No. 2, pp. 307–326. https://doi.org/10.1016/0021-9991(87)90060-X.

Bowers, E. C., 1989. The mathematical formulation of non-linear wave forces on ships. *Report no. SR193. Hydraulic Research Limited*, Wallingford, p. 48

Burmeister, H. C., Walther, L., Jahn, C., Toter, S. and Froese, J., 2014. Assessing the frequency and material consequences of collisions with vessels lying at an anchorage in line with IALA IWrap MkII. *TransNav, the International Journal on Marine Navigation and Safety of Sea Transportation*. Vol. 8, No. 1, pp. 61–68. https://doi.org/10.12716/1001.08.01.07.

Campos, R. M. and Guedes Soares, C., 2016. Comparison of HIPOCAS and ERA wind and wave reanalyses in the North Atlantic Ocean. *Ocean Engineering*. Vol. 112, pp. 320–334. https://doi.org/10.1016/j.oceaneng.2015.12.028.

Chai, T., Weng, J. and Xiong, D., 2017. Development of a quantitative risk assessment model for ship collisions in fairways. *Safety Science*. Vol. 91, pp. 71–83. https://doi.org/10.1016/j.ssci.2016.07.018.

Chen, C., Sasa, K., Ohsawa, T., Kashiwagi, M., Prpić-Oršić, J. and Mizojiri, T., 2020. Comparative assessment of NCEP and ECMWF global datasets and numerical approaches on rough sea ship navigation based on numerical simulation and shipboard measurements. *Applied Ocean Research*. Vol. 101, 102219. https://doi.org/10.1016/j.apor.2020.102219.

Chen, C., Sasa, K., Prpić-Oršić, J. and Mizojiri, T., 2021. Statistical analysis of waves' effects on ship navigation using high-resolution numerical wave simulation and shipboard measurements. *Ocean Engineering*. Vol. 229, 108757. https://doi.org/10.1016/j.oceaneng.2021.108757.

Chen, S. T. and Wang, Y. W., 2020. Improving coastal ocean wave height forecasting during typhoons by using local meteorological and neighboring wave data in support vector regression models. *Journal of Marine Science and Engineering*. Vol. 8, No. 3, 149. https://doi.org/10.3390/jmse8030149.

CNN. 2021. Everything you're waiting for is in these containers. https://edition.cnn.com/2021/10/20/business/la-long-beach-port-congestion-problem-national-impact/index.html. (accessed on 03 Feb 2022).

Coldwell, T. G., 1983. Marine traffic behaviour in restricted waters. *Journal of Navigation*. Vol. 36, No. 3, pp. 430–444. https://doi.org/10.1017/S0373463300039783.

Corbett, J. J., Winebrake, J., Endresen, O., Eide, M., Dalsøren, S., Isaksen, I. S. and Sørgård, E., 2010. International Maritime Shipping: The impact of globalisation on activity levels, in

Globalisation, Transport and the Environment, *OECD Publishing*, Paris, pp.55-80. https://doi.org/10.1787/9789264072916-5-en.

Cummins, W. E., 1962. The impulse response function and ship motions. *Schiffstechnik*, *Bd.* 9, *Heft* 47, pp.101-109.

Debnath, A. and Chin, H., 2016. Modelling collision potentials in port anchorages: Application of the Navigational Traffic Conflict Technique (NTCT). *Journal of Navigation*. Vol. 69, No. 1, pp. 183–196. https://doi.org/10.1017/S0373463315000521.

Du, W., Li, Y., Zhang, G., Wang, C., Chen, P. and Qiao, J., 2021. Estimation of ship routes considering weather and constraints. *Ocean Engineering*. Vol. 228, 108695. https://doi.org/10.1016/j.oceaneng.2021.108695.

Ducruet, C., 2020. The geography of maritime networks: a critical review, *Journal of Transport Geography*. Vol. 88, 102804. https://doi.org/10.1016/j.jtrangeo.2020.102824.

EMSA (European Maritime Safety Agency), 2020. Annual Overview of Marine Casualties and Incidents, Lisbon, Portugal, 147p. https://www.emsa.europa.eu/newsroom/latest-news/item/4266-annual-overview-of-marine-casualties-and-incidents-2020.html.

Figuero, A., Sande, J., Peña, E., Alvarellos, A., Rabuñal, J. R. and Maciñeira, E., 2019. Operational thresholds of moored ships at the oil terminal of inner port of A Coruña (Spain), *Ocean Engineering*. Vol. 172, pp. 599–613. https://doi.org/10.1016/j.oceaneng.2018.12.031.

Fujii, J. and Tanaka, K., 1971. Traffic capacity. *Journal of Navigation*, Vol. 24, No. 4, pp.543-552. https://doi.org/10.1017/S0373463300022384.

Gao, X. and Makino, H., 2017. Analysis of anchoring ships around coastal industrial complex in a natural disaster. *Journal of Loss Prevention in the Process Industries*. Vol. 50, Part B, pp. 355–363. https://doi.org/10.1016/j.jlp.2016.12.003.

Girolamo, P. D., Risio, M. D., Beltrami, G. M., Bellotti, G. and Pasquali, D., 2017. The use of wave forecasts for maritime activities safety assessment. *Applied Ocean Research*. Vol. 62, pp. 18–26. https://doi.org/10.1016/j.apor.2016.11.006.

Hansen, M., Jensen, T., Lehn-Schioler, T., Melchild, K., Rasmussen, F. and Ennemark, F., 2013. Empirical ship domain based on AIS data. *Journal of Navigation*. Vol. 66, pp. 931–940. https://doi.org/10.1017/S0373463313000489.

Im, N. and Luong T. N., 2019. Potential risk ship domain as a danger criterion for real-time ship collision risk evaluation. *Ocean Engineering*. Vol. 194, 106610. https://doi.org/10.1016/j.oceaneng.2019.106610.

Inoue, K., 1981. An investigation on reducing cable tension caused by swing motion of ship moored at single anchor in wind-I: On the factors affecting the magnitude of cable tension. *The Journal of Japan Institute of Navigation*. Vol. 65, pp. 1–12. https://doi.org/10.9749/jin.65.1. (In Japanese).

Jing, Q., Sasa, K., Chen, C., Yin, Y., Yasukawa, H. and Terada, D., 2021. Analysis of ship maneuvering difficulties under severe weather based on onboard measurements and realistic simulation of ocean environment. *Ocean engineering*. Vol. 221, 108524. https://doi.org/10.1016/j.oceaneng.2020.108524.

John, F., 1950. On the motion of floating bodies II. *Communications on Pure and Applied Mathematics*. Vol. 3, No. 1, pp. 45–101. http://doi.org/10.1002/cpa.3160030106.

Kearon, J., 1977. Computer programs for collision avoidance and traffic keeping, *Conference on Mathematical Aspects on Marine Traffic*, London, United Kingdom, pp.229-242.

Kikutani, H., Tsuruta, S., Fukutani, T., 1983. Experimental and analytical study on the dynamic tension of mooring chain. *The Journal of Japan Institute of Navigation.* Vol. 69, pp. 17–23. https://doi.org/10.9749/jin.69.17. (In Japanese).

Kubo, M., Sakakibara, S., 1999. A Study on time domain analysis of moored ship motion considering harbor oscillations. *Proceedings of the 9th International Offshore and Polar Engineering Conference*, France, pp.574-581. https://www.onepetro.org/conference-paper/ISOPE-I-99-309.

Liu, D. and Shi, G., 2020. Ship collision risk assessment based on collision detection algorithm. *IEEE Access*. Vol. 8, pp. 161969–161980. https://doi.org/10.1109/ACCESS.2020.3013957.

Liu, Z., Wu, Z. and Zheng, Z., 2019. A novel framework for regional collision risk identification based on AIS data. *Applied Ocean Research.* Vol. 89, pp. 261–272. https://doi.org/10.1016/j.apor.2019.05.020.

Liu, Z., Wu, Z. and Zheng, Z., 2020. A novel model for identifying the vessel collision risk of anchorage. *Applied Ocean Research*. Vol. 98, 102130. https://doi.org/10.1016/j.apor.2020.102130.

Lee, S. W., Sasa, K., Aoki, S., Yamamoto, K. and Chen C., 2021. New evaluation of ship mooring with friction effects on mooring rope and cost-benefit estimation to improve port safety. *International Journal of Naval Architecture and Ocean Engineering*. Vol. 13, pp. 306–320. https://doi.org/10.1016/j.ijnaoe.2021.04.002.

Lu, L. F., Sasa, K., Sasaki, W., Terada, D., Kano, T. and Mizojiri, T., 2017. Rough wave simulation and validation using onboard ship motion data in the southern hemisphere to enhance ship weather routing. *Ocean Engineering*. Vol. 144, pp. 61–77. https://doi.org/10.1016/j.oceaneng.2017.08.037.

Lu, Y. and Bai, C., 2015. Dragging anchor event and theoretical verification of single mooring ship. *Proceedings of the 9th International Conference on Frontier of Computer Science and Technology, FCST 2015*, pp. 209–213. https://doi.org/10.1109/FCST.2015.16.

Luong, T. N., Hwang, S. and Im, N., 2021. Harbour Traffic Hazard Map for real-time assessing waterway risk using Marine Traffic Hazard Index. *Ocean Engineering*. Vol. 239, 109884.

https://doi.org/10.1016/j.oceaneng.2021.109884.

MAIA (Marine Accident Inquiry Agency), 2006. Collection of Maritime Disaster Typhoon and Maritime Disaster, 131p. http://www.mlit.go.jp/jtsb/kai/bunseki/bunsekikohosiryo/no6_taihu/taihutokainantop.htm. (In Japanese).

MLIT (Ministry of Land, Infrastructure, Transport and Tourism), 2009. Technical standards and commentaries for port and harbour facilities in Japan. Translated and edited by The Overseas Coastal Area Development Institute of Japan, Tokyo, 981p. http://ocdi.or.jp/en/technical-st-en.

Nakajima, T., Motora, S. and Fujino, M., 1982. On the dynamic analysis of multi-component mooring lines. *Proceedings of the Annual Offshore Technology Conference*. pp. 105–110. https://doi.org/10.4043/4309-MS.

Natskår, A., Moan, T. and Alvær, P., 2015. Uncertainty in forecasted environmental conditions for reliability analyses of marine operations. *Ocean Engineering*. Vol. 108, pp. 636–647. https://doi.org/10.1016/j.oceaneng.2015.08.034.

Pietrzykowski, Z. and Uriasz, J., 2009. The ship domain – A criterion of navigational safety assessment in an open sea area. *Journal of Navigation*. Vol.62, pp. 93–108. https://doi.org/10.1017/S0373463308005018.

Pietrzykowski, Z. and Wielgosz, M., 2021. Effective ship domain – Impact of ship size and speed. *Ocean Engineering*. Vol. 219, 108423. https://doi.org/10.1016/j.oceaneng.2020.108423.

Plessas, T., Kanellopoulou, A., Zaraphonitis, G., Papanikolaou, A. and Shigunov, V., 2018. Exploration of design space and optimisation of RoPax vessels and containerships in view of EEDI and safe operation in adverse sea conditions. *Ocean Engineering*. Vol. 162, pp. 1–20. https://doi.org/10.1016/j.oceaneng.2018.05.022.

Qinetiq, Lloyd's Register, and Univ. of Strathclyde, 2013. Global marine trends 2030. pp. 1–144.

Sasa, K. and Incecik, A., 2012. Numerical simulation of anchored ship motions due to wave and wind forces for enhanced safety in offshore harbor refuge. *Ocean Engineering*. Vol. 44, pp. 68–78. https://doi.org/10.1016/j.oceaneng.2011.11.006.

Sasa, K., Chen, C., Shiotani, S., Ohsawa, T., and Terada, D., 2014. Numerical analysis of failed forecasts of waves under low pressures from viewpoint of ship operation, *Proceedings of the 33rd International Conference on Ocean, Offshore and Arctic Engineering*, *OMAE2014*, pp. 1–8. https://doi.org/10.1115/OMAE2014-23876.

Sasa, K., Mitsui, M., Aoki, S. and Tamura, M., 2018. Current analysis of ship mooring and emergency safe system. *Journal of Japan Society of Civil Engineers, Ser. B2 (Coastal Engineering)*. Vol.74, No.2, pp.1399-1404. http://doi.org/10.2208/kaigan.74.I_1399. (In Japanese).

Sasa, K., Aoki, S., Fujita, T. and Chen, C., 2019. New evaluation for mooring problem from cost-benefit effect. *Journal of Japan Society of Civil Engineers, Ser. B2 (Coastal Engineering)*. Vol. 75, No. 2, pp. 1243–1248. http://doi.org/10.2208/kaigan.75.I_1243. (In Japanese).

Sasa, K., Chen, C., Fujimatsu, T., Shoji, R. and Maki, A., 2021. Speed loss analysis and rough wave avoidance algorithms for optimal ship routing simulation of 28,000-DWT bulk carrier. *Ocean Engineering*. Vol. 228, 108800. https://doi.org/10.1016/j.oceaneng.2021.108800.

Sharpey-Schafer, J. M., 1954. Anchor Dragging. *Journal of Navigation*. Vol. 7, No. 3, pp. 290–300. https://doi.org/10.1017/S0373463300020968.

Shiraishi, S., Kubo, M., Sakakibara, S. and Sasa, K., 1999. Study on numerical simulation method to reproduce long-period ship motions. *Proceedings of the 9th International Offshore and Polar Engineering Conference*, France, pp. 536–543. https://www.onepetro.org/conference-paper/ISOPE-I-99-304.

Stopa, J. E. and Cheung, K. F., 2014. Intercomparison of wind and wave data from the ECMWF Reanalysis Interim and the NCEP Climate Forecast System Reanalysis. *Ocean Modelling*. Vol. 75, pp. 65–83. https://doi.org/10.1016/j.ocemod.2013.12.006.

Sugomori, M., 2010. An empirical study on the need for anchor operation education and training. *World Maritime University Dissertations*. 418, http://commons.wmu.se/all_dissertations/418.

Tam, C. and Bucknall, R., 2010. Collision risk assessment for ships. *Journal of Marine Science and Technology*. Vol. 15, No. 3, pp. 257–270. https://doi.org/10.1007/s00773-010-0089-7.

The New York Times. 2021. 'I've Never Seen Anything Like This': Chaos Strikes Global Shipping. https://www.nytimes.com/2021/03/06/business/global-shipping.html. (accessed on 03 Feb 2022).

Tolman. H. L., 1989. The numerical model WAVEWATCH: a third-generation model for hindcasting of wind waves on tides in shelf seas. Faculty of Civil Engineering, Delft University of Technology.

Tolman. H. L., 2014. User manual and system documentation of WAVEWATCH III, Version 4.18, p. 282, *National Oceanic and Atmospheric Administration/National Weather Service/National Centers for Environmental Prediction (NOAA/NWS/NCEP)*. Technical Note.

UNCTAD (United Nations Conference on Trade and Development), 2020. Review of maritime transport. New York; Geneva, 146p. https://doi.org/10.18356/9789210052719.

Ura, T. and Toshim, T, 1980. A basic study on the transient behaviors of moored structures on the sea. *Journal of the Society of Naval Architects of Japan*. Vol. 148, pp. 121–127. https://doi.org/10.2534/jjasnaoe1968.1980.148_121. (in Japanese).

Van der Molen, W., Monardez, P. and van Dongeren, A. P., 2006. Numerical simulation of long-period waves and ship motions in Tomakomai port, Japan. *Coastal Engineering Journal*. Vol. 48, pp. 59–79. https://doi.org/10.1142/S0578563406001301.

Ventikos, N. P., Koimtzoglou, A. and Louzis, K., 2015. Statistics for marine accidents in adverse weather conditions. Maritime Technology and Engineering – Guedes Soares & Santos (Eds). Taylor & Francis Group, London. pp. 243–251. https://doi.org/10.1201/b17494

Walton, T. S. and Polachek, H., 1960. Calculation of transient motions of submerged cables. *Journal of Mathematics of Computation*. Vol.14, No.69, pp.27–46. https://doi.org/10.2307/2002982.

Wang, Y. and Chin, H., 2016. An empirically-calibrated ship domain as a safety criterion for navigation in confined waters. *Journal of Navigation*. Vol. 69, pp. 257–276. https://doi.org/10.1017/S0373463315000533.

Yeo, G. T., Roe, M. and Soak, S. M., 2007. Evaluation of the marine traffic congestion of north harbor in Busan port. *Journal of Waterway, Port, Coastal, and Ocean Engineering*. Vol.133, No.2, pp.87-93. https://doi.org/10.1061/(asce)0733-950x(2007)133:2(87).

Zhang, C., Zhang, D., Zhang, M. and Mao, W., 2019. Data-driven ship energy efficiency analysis and optimization model for route planning in ice-covered Arctic waters. *Ocean Engineering*. Vol.186, 106071. https://doi.org/10.1016/j.oceaneng.2019.05.053.

Zhang, P. and Zhao, J., 2013. The obligations of an anchored vessel to avoid collision at sea. *Journal of Navigation*. Vol. 66, No. 3, pp. 473–477. https://doi.org/10.1017/S0373463313000088.

Zhao, Y., Li, W. and Shi, P., 2016. A real-time collision avoidance learning system for Unmanned Surface Vessels. *Neurocomputing*. Vol. 182, pp. 255–266. https://doi.org/10.1016/j.neucom.2015.12.028.

Zhen, R., Riveiro, M. and Jin, Y., 2017. A novel analytic framework of real-time multi-vessel collision risk assessment for maritime traffic surveillance. *Ocean Engineering*. Vol. 145, pp. 492–501. https://doi.org/10.1016/j.oceaneng.2017.09.015.

Zou, Y., Shen, C. and Xi, X., 2012, Numerical simulations on the motions of anchored capesize ships. *Journal of Navigation*. Vol. 65, No. 1, pp. 145–158. https://doi.org/10.1017/S0373463311000580.